DEVELOPMENT OF SHAPE MEMORY POLYMERS FOR MINIMALLY-INVASIVE VASCULAR CONSTRUCTS

By

Timothy Charles Boire

Thesis

Submitted to the Faculty of the

Graduate School of Vanderbilt University

In partial fulfillment of the requirements

for the degree of

MASTER OF SCIENCE

In

Biomedical Engineering

December, 2013

Nashville, Tennessee

Approved:

Hak-Joon Sung, Ph.D.

Craig Duvall, Ph.D

To my parents Judy and Dan, who gave me so many opportunities in life to succeed

and to my family, Nicole, Nathan, Jeremy, Jason, Grandma and Grandpa Boire, Grandma and Grandpa Lovely, and my incredibly supportive friends through the years

ACKNOWLEDGEMENTS

First and foremost, I would like to thank Dr. Hak-Joon Sung. Without his guidance, support, and friendship this project would not be possible. I would also like to thank Dr. Raul Guzman and Dr. Andre Mitchell for providing us with the resources and the means to conduct *in vivo* rat experiments with our materials. I also owe much gratitude to Dr. Scott Guelcher for providing all of the resources necessary to conduct this study. This work would not be possible without his generosity. I would also like to thank Dr. Craig Duvall for his everyday advice and friendship.

Additionally, I would like to thank all my fellow research members. Special thanks go to Dr. Mukesh Gupta for his innovation and expertise in polymer chemistry. Without his contributions, this work may not have been possible. I would also like to thank Angela Zachman, Sue Hyun-Lee, Spencer Crowder, Lucas Hofmeister, Rutwick Rath, Brian Evans, John Martin, John Page, Elizabeth Adolph, Martina Miteva, and Kelsey Beavers for their help with experiments, day to day lab work, and support the past two and a half years. I don't know where I would be without all of my great labmates. I would also like to thank all of my undergraduate assistants Joshua Stewart, James Taylor, Brandon Lynch, David Dubetz, and Sanjid Md. Halim for their help with performing laboratory experiments and camaraderie the past two years.

NMR spectroscopy was conducted in the NMR Small Molecule Facility. Photolithography was conducted in the Vanderbilt Institue for Integrative Biosystems Research and Education (VIIBRE) facilities. Confocal imaging was performed through resources in the VUMC Cell Imaging Shared Resources (supported by NIH Grants CA68485, DK20593, DK58404, HD15052, DK59637, and Ey008126). This work was supported by NSF CAREER CBET 1219573.

LIST OF TABLES

LIST OF FIGURES

Supplementary Figure Page

TABLE OF CONTENTS

Appendix Page

CHAPTER I

INTRODUCTION

Shape Memory Polymers

Introduction

Shape memory polymers (SMPs) are a class of "smart" materials that respond to specific stimuli by changing shape. A tremendous amount of attention has been given to these materials over the last two decades owing to the potential utility of this unique property in a wide variety of industrial and biomedical applications [1]. Temperature (i.e. heating above glass transition (T_g) or melting temperature (T_m) is the most common stimulus for shape recovery, although other SMPs have emerged that are actuated by light [2, 3], magnetic fields [4], electricity [5, 6], moisture [7, 8], and pH [9]. SMPs can be programmed into a temporary shape by mechanical deformation and maintain this shape until triggered by this specific external stimulus. It is only at this point of stimulation that the material reverts back to its original, permanent shape. This ability to be ***fixed*** into a temporary shape and ***recover*** the original shape in response to a specific stimulus can be described accordingly as the shape memory effect (SME). SME also describes the behavior of other shape memory materials (SMMs) such as shape memory alloys (SMAs).

The first-recorded observation of the SME was in 1932 with a SMA by Chang and Read [10] and applications of SMPs that employed this effect such as heat-shrinkable tubing were commercially available by the 1960's. However, the first official use of the SMP term is believed not to have occurred until 1984. At this time, the CDF Chimie Company in France developed a poly(norbornene) based SMP [11]. Upon commercialization of this product in Japan, two other polyene-based SMPs, poly(trans-isoprene) and poly(styrene-butadiene), emerged from Japan [11]. It was not until the 1990's, however, that scientific research on the SME in polymers began in earnest, upon the advent of segmented polyurethane–based SMPs by Mitsubishi Heavy Industries Ltd. [12]. The expansion in SMP research at this time can be attributed to the vast utility of polyurethane in industrial applications and the relative ease with which its thermal and mechanical properties can be tuned [12]. Then in 2002, Lendlein et al demonstrated the use of a SMP network (comprised of oligo(***ε***-caprolactone)diol/oligo(*p*-dioxanone)diol blend) as a self-tightening suture for minimally invasive surgery, which sparked the exponential growth in interest with SMPs that persists today [12, 13].

Mechanism

Regardless of the mode of actuation, SMP networks must possess both mobile and physically-anchored domains to exhibit the SME [12]. As the term implies, the mobile or "soft" domains are the network domains that move in parallel with the network's net movements. Mobile domains are amorphous or semicrystalline polymers termed ***molecular switches*** or ***stimuli-sensitive domains*** that mobilize to enable mechanical deformation into a temporary shape and remobilize during shape recovery ***[1]***. Physical anchor or "hard" domains are almost always chemical (i.e. covalent bonds) or physical (i.e. associations based on phase separation and domain orientation) primary crosslinks (Figure 1), and are

termed ***netpoints*** [14] ***[1]***. These netpoints prevent irreversible, plastic deformation (i.e. chain slippage) from occurring during both the fixity and recovery steps, storing strain energy during mechanical deformation and releasing this amount of energy during shape recovery. Moreover, secondary crosslinks relating to associations between side chains are formed in the reduced kinetic environment (e.g. lower temperature) of the fixation step ("Pre-deformed shape" in Figure 1A), which further stabilizes or fixes the polymer in its deformed, temporary shape [14]. Once the appropriate stimulus is applied (e.g. heat above T_m or T_g), the molecular switch domains remobilize and cause the secondary crosslinks to dissociate. The strain energy that was stored during deformation by the primary netpoints and secondary crosslinks is released, and in the absence of applied mechanical force, the SMP will revert back to its original shape. Owing to the netpoints or hard domains, the mobility of the molecular switch segments are able to dominate chain slippage events in the recovery process of the SME [1].

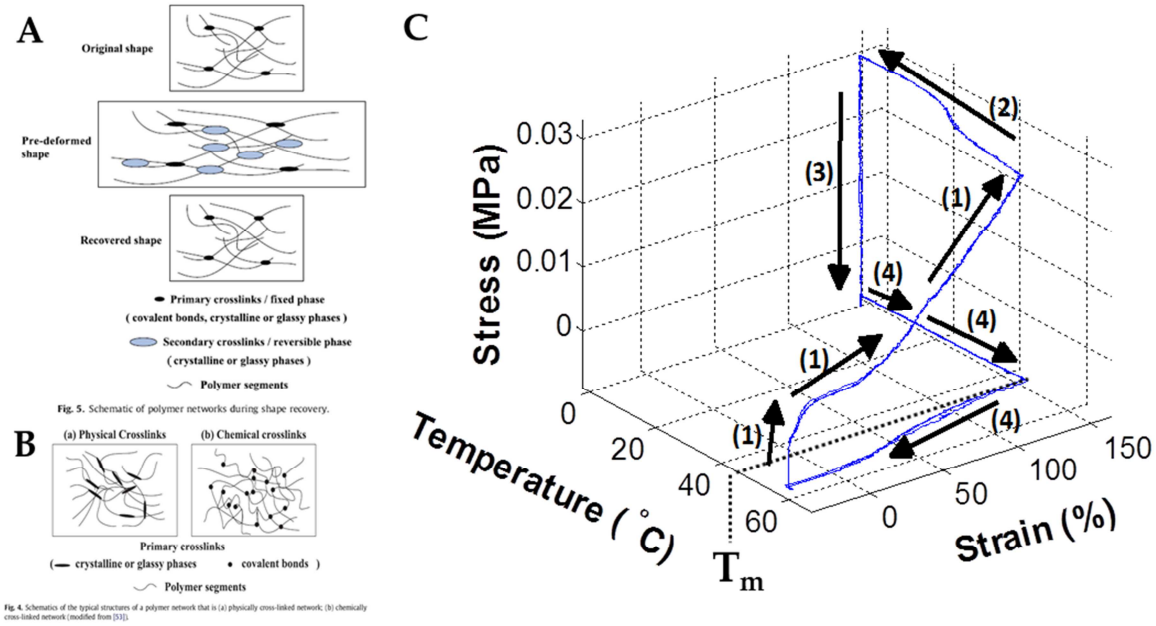

Figure 1: SME explained by crosslinks and thermomechanical cycling. (A) and (B) are from Leng et al [14]. (A) Role of primary and secondary crosslinks in shape fixity and shape recovery for a covalently crosslinked SMP network. (B) The distinction between physically and chemically cross-linked SMP networks is based on the nature of the crosslinks (covalent bonds or phase separation) [14]. (C) 3D plot of stress, strain (i.e. deformation), and temperature for a thermo-responsive SMP being manipulated through a cycle of shape change. (1) Mechanical deformation into temporary shape. (2) Cooling below T_m. (3) Removal of force load to create temporary shape. (4) Heating above T_m and return to original, permanent shape [15].

The most dominant and illustrative example of the SME in polymers are thermo-responsive SMPs where the driving force for shape recovery is temperature. These polymers possess at least one distinct thermal transition temperature (T_{trans}), either a glass-transition (T_g) or melting temperature (T_m). Once the physical or chemical cross-links of the material are defined to obtain the stable, permanent shape, the polymer is (Figure 1C) 1) heated above its T_{trans} and deformed into its temporary shape by an applied force. Next the polymer is 2) cooled below it T_{trans} with the applied force maintained, then 3) the applied force is unloaded at this lower temperature. At this point, the polymer is fixed into its temporary shape as the molecular switch segment is essentially frozen at the lower temperature and further stabilized by secondary crosslinks between the polymer chains. Lastly, 4) the polymer is heated above its transition temperature to recover its original shape. This recovery is made possible by the increased mobility of the

molecular switch segment above the transition temperature and subsequent disassociation of secondary crosslinks, while the netpoints prevent chain slippage.

The kinetics underlying the SME can be explained by thermodynamics. The deformation step (Figure 1C, 1)) reduces the entropy of the polymer as fewer conformations are possible in the strained state (Boltzmann entropy equation, S = k*W; S = entropy, k = Boltzmann constant, W = probability of conformations) [1]. When the polymer is cooled in step 2 and the force released in step 3, the polymer does not revert back to its more favorable, permanent shape as an elastic material normally would. This is because the restoring force to drive the shape back to its original conformation is less than the force required to mobilize the entangled polymer chains in this reduced temperature, reduced entropy state. However, as the temperature is increased above T_{trans} in step 4, the entropic elasticity becomes sufficient enough to overcome the chain entanglements and recover the permanent, higher entropy, more disordered state. Essentially the chain entanglements act as secondary physical cross-links to enable fixation of a temporary shape at lower temperature, while the recovery of the permanent shape is made possible through the primary cross-links or netpoints which prevent slippage of the polymer chains. just as cross-links do so in elastomers (entropic elasticity).

This description of the underlying mechanism responsible for SME in polymers holds true for SMPs actuated by other types of energy such as magnetism, electricity, light and pH as they are mostly examples of indirect heating. For example, magneto-responsive SMPs are usually comprised of polymers with superparamagnetic iron oxide nanoparticles and an inductive coil. Upon exposure to an alternating current (AC), a magnetic field is produced which induces a current through the SMP and is dissipated as heat via inductive heating, causing $T > T_{trans}$ and recovery of shape [4]. Similarly, polymers with conductive material embedded in them such as nanotubes can be exposed to a current that dissipates as heat and causes the SME in thermo-responsive SMPs. Light-activated SMPs can also be derived where high intensity light indirectly produces heat [14]. On a similar note, polyurethanes wetted with water have been shown to exhibit reduced T_g's and thus require little to no direct heating for SME [7].

Classification of Thermo-responsive SMPs

As has already been suggested, SMPs actuated by other forms of energy are merely derivatives of the same thermally-derived mechanism, so it is imperative to further classify this important set of polymers based on the type of cross-links formed and the type of T_{trans}. Thermo-responsive SMPs are either: (I) chemically cross-linked glassy thermosets ($T_{trans} = T_{g),}$ (II) chemically cross-linked semicrystalline rubbers ($T_{trans} = T_{m)}$, (III) physically cross-linked amorphous thermoplastics ($T_{trans} = T_{g)}$, and (IV) physically cross-linked semicrystalline block copolymers ($T_{trans} = T_m$) [16]. Class I and III SMPs tend to display a higher modulus and wider transition temperatures than SMPs based on T_m, which may affect the rate of recovery [16]. Chemically cross-linked polymers tend to display higher shape fixity and shape recovery as their netpoints are better defined [16].

Other interesting types of SMPs

There are several other types of SMPs and SMMs that are unique in their method of stimulation and their ability to form multiple temporary and permanent shapes. One unique method of stimulation incorporated cinnamic groups which afforded the ability of the polymer to be fixed in its strained state via UV cross-linking during straining (Figure 2) [2]. This temporary shape was thermally stable beyond its transition temperature. The permanent shape could be selectively recovered by exposing the polymer to higher energy (lower wavelength) UV light, which cleaved the photosensitive bonds that were holding the

polymer in its original conformation. A potential improvement upon this technology for biomedical applications is the selective employment and application of such a device at a higher wavelength, as UV light can trigger reactive oxygen species (ROS) production which can lead to damaged tissue [17].

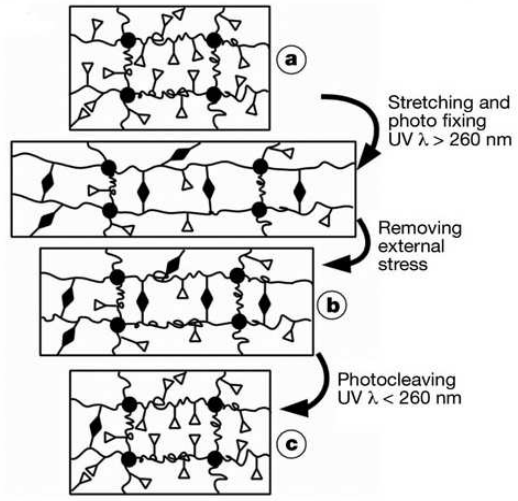

Figure 2: Schematic of a light-activated SMP that was cured and cleaved with UV light. From Lendlein et al [2].

Another interesting class of SMPs to note is multi-shape memory polymers. In one such polymer system, multiple shapes could be programmed by applying different radiofrequencies to a SMP containing spatially separated iron oxide nanoparticles and carbon nanotubes [18]. In a more prominent example, a proton conducting ionomer was utilized that possessed multiple discrete reversible phase transitions which resulted in multiple temporary and memorized shapes [19]. The multi-shape memory effect was made possible in this case because of the broad glass transition, which can be thought of as an infinite number of small transitions. Various temporary shapes were derived, and three different strains could be recovered with high shape recovery based on the amount of heating. It is difficult to foresee deployment of a multi-shape device in biomedical applications in the near future due to the difficulty in controlling shape change in the dynamic environment of the body. However, it proves useful as a means to study the underlying mechanisms that govern shape memory behavior in their relation to thermal and mechanical properties to improve control of shapes in SMPs.

Applications

Current and potential applications of SMPs are wide-ranging, and include self-deployable spacecraft structures, smart fabrics, heat-shrinkable tubes, intelligent medical devices, cell-active substrates, and for minimally-invasive surgical applications [1, 20-22]. Two excellent recent reviews of SMPs in biomedical applications are provided by Lendlein et al and Serraro et al [23, 24]. In the biomedical field, SMPs have been investigated for many applications including general surgery [25-28], vascular applications [29-47], urogynecology [36, 48-52], ophthalmology [53], neurology [54, 55], orthopedics [56], orthodontics [57], and gastrointestinology [52, 58-60]. Vascular applications are of particular interest to the author, and involve fasteners and stents [29, 46, 61-64], aneurysmal occlusion fillers [35, 42, 44, 65-67], microactuators for endovascular clot removal [47, 68, 69], and as drug delivery platforms [70-74]. The main advantages of SMPs in vascular applications are minimally-invasive deployment and the ability to custom-fit a shape specific to the geometry of the patient [60]. For example,

in the case of a stent, a coronary angiogram image could be processed in imaging analysis software, an algorithm could compute the optimal design of the stent based on the occlusion, and this design could be converted to a CAD drawing for 3D printing of the device. After sterilization, the SMP device could be deformed into a shape such as a thread for insertion through a catheter, and deployed to the site of interest. These capabilities may not be possible with other shape memory materials such as shape memory alloys (SMAs). Compared to SMAs, SMPs are low cost, low density, have much greater elastic deformation (greater than 200% compared to 8%), and can potentially be biocompatible and biodegradable [75]. Also, SMPs are easy to process and their properties (e.g. stiffness, T_{trans}) can be easily adjusted [75]. Despite these many attractive characteristics, few if any such devices have reached the clinic. The motivation behind the work in Chapter II is to bring SMPs closer to a clinical reality.

CHAPTER II

DEVELOPMENT OF SHAPE MEMORY POLYMERS FOR MINIMALLY INVASIVE VASCULAR CONSTRUCTS

Introduction

Carotid artery disease (CAD) is responsible for ~20% of strokes, the third leading cause of death in the United States, and often coexists in patients with coronary artery disease as well as peripheral artery disease [76]. CAD is characterized by the narrowing or stenosis of the carotid artery, and is the result of progressive atherosclerosis. As calcium and cholesterol deposits buildup along the arterial wall, an atherosclerotic plaque forms and results in a condition of oscillatory flow with overproduction of matrix metalloproteinases (MMPs). Due to MMP-mediated degradation at the shoulder regions, the plaque becomes unstable and eventually undergoes rupture, leading to vessel occlusion and downstream tissue necrosis due to deprivation of oxygen and nutrients. Finally this process can lead to transient ischemic events or stroke.

When carotid artery stenosis is detected by techniques such as duplex ultrasonography, carotid endarterectomy (CEA) is the most common treatment option. CEA is a highly invasive, expensive surgical technique in which the common carotid artery is cross-clamped before opening the artery and excising the plaque. While it has proven effective in treating symptomatic carotid stenosis, its benefit in asymptomatic patients remain controversial and it is associated with significant risks, including myocardial infarction, cranial nerve injury, and wound infection [77-80]. As a result, minimally invasive techniques such as balloon angioplasty and stenting have been pursued. While stenting was shown to be equivalent to CAE in a large clinical study [77], it cannot be applied to complex arterial anatomies and has higher rates of perioperative stroke [77, 81]. For complex lesions and aneurysmal treatment, autologous venous or arterial sources are employed in carotid artery bypass grafting with mixed results [82-84]. Although arterial grafts have demonstrated greater efficacy than saphenous venous grafts, they have limited availability, especially for CAD patients with other cardiovascular diseases. Moreover, implementation of either source requires highly invasive and costly surgery [83, 85].Thus, there is a great need to develop auxiliary or alternative minimally-invasive treatment modalities that are effective, simple, and applicable to complex anatomical features that cannot be treated by endovascular techniques.

One potential approach is to provide a functionalized conduit that can maintain normal blood flow to the brain while regenerating the diseased, occluded tissue. Degradable polymers can be progressively replaced by regenerating tissue and eventually become completely biological grafts [86-88]. Poly(ε-caprolactone) (PCL) is a biocompatible, slowly biodegradable polymer with excellent elasticity and toughness that is FDA-approved for use as forms of resorbable sutures, tissue engineered scaffolds, and drug delivery vehicles [89]. Small diameter (2 mm) electrospun PCL grafts demonstrated improved healing, endothelialization, and angiogenesis in comparison to the non-biodegradable expanded polytetrafluoroethylene (PTFE) grafts after 24 weeks in the rat abdominal aorta [90]. However, PCL still degrades too slowly and is too bio-inert to exhibit sufficient tissue integration and regeneration on its own. As a promising alternative, Zachman et al demonstrated that soft tissue regeneration was promoted when a polymer scaffold embedded in a collagen gel containing pro-angiogenic C16 and anti-inflammatory peptides Ac-SDKP was implanted in a dorsal region of mice [91]. It was found that C16, derived from laminin-1, and Ac-SDKP, derived from thymosin β-4, promoted angiogenesis while minimizing inflammatory responses upon release from a collagen gel.

To reduce surgical complexity and enable minimally invasive deployment, PCL can be modified and crosslinked to create a shape memory polymer (SMP) network. SMPs are materials with the unique capability of being *fixed* into a temporary shape and *recover* their original, permanent shape in response to a certain stimulus such as temperature, light [2, 3], magnetic fields [4], moisture [7, 8], or pH [9]. For this application, it is desired to fix thermo-responsive SMPs into an elongated, thread-like shape for catheter-mediated insertion and deployment, and recover a tubular shape mimetic of an artery. PCL SMPs terminally functionalized with methacrylate groups possess excellent shape memory properties [92], but their transition temperature (T_m ~ 50^{o}C) is too high for physiological applications. Common methods to reduce the T_m of PCL closer to 37^{o}C include incorporation of rigid components, blending, branching, and molecular weight alteration [13, 93-97]. In this study, copolymerization with a novel hydrophobic monomer, α-allyl carboxylate-ε-caprolactone (**ACCL**), was used to create poly(ε-caprolactone)-co-(α-allyl carboxylate-ε-caprolactone) [*x*%PCL-*y*%ACPCL (*x* and *y*: molar ratio)], a new class of SMPs. This copolymerization strategy enables precise control of material properties by tuning molar composition and molecular weight. Furthermore, the presence of pendant allyl groups along the polymer chains obviates the need for a functionalization step to create covalently crosslinked SMP networks. The crosslinked networks can be fabricated into tubes, deformed into an elongated thread-shape, and implanted and sutured on either side of the occlusion in a minimally invasive manner (Figure 3).

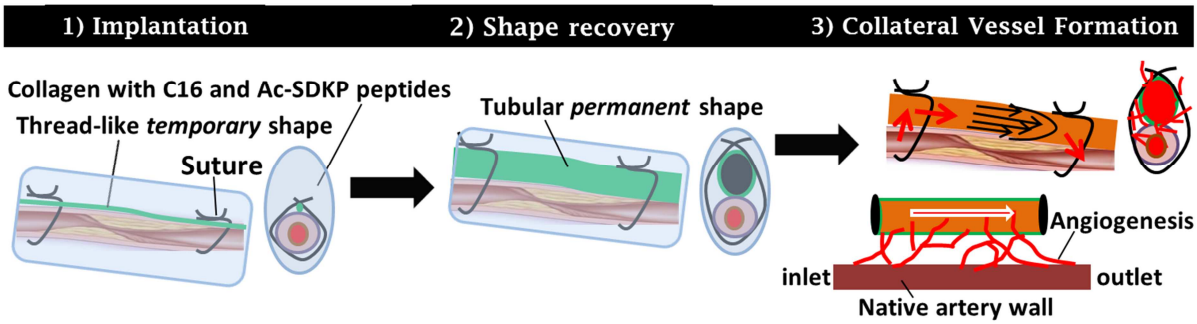

Figure 3: Schematic demonstrating blood bypassing an occlusion site using a SMP construct. 1) SMP is implanted in thread-like shape across the entire occluded area, sutured on both sides of the occlusion, and treated with a collagen gel containing pro-angiogenic and anti-inflammatory peptides C16 and Ac-SDKP, respectively. 2) The SMP construct recovers its tubular permanent shape. 3) Over the course of 2 weeks capillary growth and anastomosis with the SMP construct are induced, thereby providing a conduit for blood flow past the occlusion. This revascularization strategy could potentially provide adequate flow downstream of the occluded regions and rescue the ischemic area.

This study validates that producing this novel x%PCL-y%ACPCL copolymer library is an effective strategy in creating SMPs with reduced melting temperatures around 37 ^{o}C and fine-tuning of mechanical and shape memory properties. *In vitro* degradation and biocompatibility were also assessed for various film constructs before testing the utility of tubular implants in a rat model of occlusive (double ligated) carotid arteries. Through this MS thesis study, the SMP constructs were shown capable of integrating into the native artery, regenerating diseased tissue, and being deployed in a minimally invasive way.

Methods

Materials

Anhydrous tetrahydrofuran (THF), ε-caprolactone, lithium diisopropylamide (LDA) (2 M in THF/*n*-heptane/ethylbenzene), PCL (70 – 90 kDa), allyl chloroformate, ethyl acetate, hexanes, calcium hydride, ammonium chloride, sodium sulfate, 1,6-hexanediol, $Zn(Et)_2$ (15 wt% in toluene), $Sn(Oct)_2$, dichloromethane (DCM), ethanol, and diethyl ether were purchased from Sigma (St. Louis, MO). All reagents were used as purchased except for ε-caprolactone, which was distilled via vacuum distillation using calcium hydride as a desiccant.

Synthesis and characterization of α-allyl carboxylate-ε-caprolactone (ACCL) monomer

ACCL was synthesized by adopting a similar method described for α-benzyl carboxylate-ε-caprolactone synthesis [98]. In a dried, sealed 500 mL round bottom flask equipped with a three-way stopcock, LDA (125 ml of 2 M in THF/n-heptane/ethylbenzene; 250 mmol) was slowly added to anhydrous THF (200 mL) in the presence of nitrogen under vigorous stirring at -30 ^{o}C. The solution was cooled to -78℃. Next, ε-caprolactone (13.9 mL; 125 mmol) was added drop-wise (~0.5 mL/min) and the temperature (-78℃) was maintained for 1 hour. The mixture was equilibrated to -30 ^{o}C and Allyl chloroformate (13.3 mL; 125 mmol) was added drop wise. This temperature (-30 ^{o}C) was strictly maintained for 30 minutes, then raised to 0 ℃, and the reaction was quenched with saturated ammonium chloride solution (30 mL). The reaction mixture was diluted with 75 ml of water and extracted three times with ethyl acetate (200 mL). The combined extracts were dried over Na_2SO_4, filtered, and evaporated by rotatory evaporation. The formation of monomer was checked by TLC in 30% ethyl acetate in hexane. The yellowish oily crude mixture was purified over a Silica Gel Premium Rf Rf (Sorbent Technologies, Norcross, GA) column using 10% ethyl acetate in hexane until all the monomer eluted out. Purified samples were combined, solvent was evaporated, and the purified monomer was placed under high vacuum. Final yield after purification was 14.3 g or 58%. ^{1}H-NMR was recorded on a Brüker 400 MHz spectrometer to confirm the conversion of ε-caprolactone to ACCL: ^{1}H NMR ($CDCl_3$, 400 MHz) δ: 5.92 (m, 1H, **CH**=CH_2), 5.31 (m, 2H, -CH=**CH_2**CH_2), 4.63 (m, 2H, -CH=CH_2**CH_2**), δ 4.20 (m, 2H, -OCH_2), 3.73 (d, 1H, -CH_2), 2.18 – 1.74 (m, 4H, -CH_2), 1.61 (m, 2H, -CH_2) ppm.

Synthesis and characterization of x%PCL-y%ACPCL polymers

Distilled ε-caprolactone and ACCL (100 mmol total) were added to 1,6-hexanediol (0.5 mmol) in a dried test tube with varying molar ratios and degassed in two freeze--thaw cycles. At 140^{o}C, $Zn(Et)_2$ (1 mmol; 15 wt% in toluene) was added and reacted for approximately 1 hour. The solution was cooled and precipitated in cold diethyl ether. The precipitated product was dried under vacuum. ^{1}H NMR ($CDCl_3$, 400 MHz) δ: 5.90 (m, 1H, **CH**=CH_2), 5.29 (q, 2H, -CH=**CH_2**CH_2), 4.62 (d, 2H, -CH=CH_2**CH_2**), 4.15 (m, 2H, -OCH_2), 3.35 (m, 1H, -CH-COOC), 2.33 (t, 2H, -CH_2), 1.95 (q, 2H, -CHC**H_2**CH_2), 1.62 (m, 4H, -CH_2), 1.39 (m, 2H, -CH_2) ppm. Molar composition was determined by the ratio of the 5.90 ppm integral, $I_{5.90}$, to the 4.15 ppm integral, $I_{4.15}$:

$$y\%ACPCL = 2 \times \frac{I_{5.90}}{I_{4.15}} \times 100\% \text{ (Equation 1)}$$

Gel permeation chromatography (GPC) was performed in THF on a Phenogel 10E3A column (Phenomenex Inc., Torrance, CA) with a RID-10A. Molecular weights were determined against poly(methyl methacrylate) standards (Agilent Technologies, Inc., Santa Clara, CA).

Synthesis and characterization of 100%PCL and 100%PCL-dimethacrylate controls

As a control, 100%PCL-dimethacrylate was prepared. First, 100%PCL was prepared as described above without any ACCL and using $Sn(Oct)_2$ as a catalyst instead of $Zn(Et)_2$. The precipitated produced (1.0 g) was methacrylate-functionalized by adding 2-isocyanatoethyl methacrylate (0.2 mL) and a catalytic amount (10 µL) of dibutyltin dilaurate at 60°C for 1 hour [99] (Appendix A). The product was washed several times with hexanes and dried under vacuum. ^{1}H NMR ($CDCl_3$): δ 6.13(s, 1H, **CH_2**=C), 5.62 (s, 1H, **CH_2**=C), 5.2 (m, 2H, -CH=**CH_2**CH_2), 4.97 (m, 1H, 0=CN**H**CH_2), 4.23 (m, 2H, -OC**H_2**CH_2), 4.06 (t, 2H, -OCH_2), 3.64 (m, 2H, -NCH_2), 2.32 (t, 2H, -CH_2), 1.94 (m, 3H, -CH_3), 1.64 (m, 2H, -CH_2), 1.39 (m, 4H, -CH_2) ppm.

SMP Film Preparation

Polymers (0.4 g) and 2,2-dimethoxy-2-phenylaceto-phenone (DMPA) (10 mg) were solubilized in dichloromethane (0.3 mL). To produce films of uniform thickness, the solution was pipetted onto stainless steel sheets (Grainger, Inc., Lake Forest, IL) and flattened with a thin film applicator (Precision Gage & Tool, Co., Dayton, OH). The thin film layer was then irradiated at 365 nm (4.89 J/cm^2; 18.1 mW/cm^2) using the Novacure 2100 Spot Curing System (Exfo Photonic Solutions, Inc., Mississauga, Ontario, Canada). Films were solvent casted overnight and placed under high vacuum for 2 hours.

Gel content

To determine the degree of crosslinking, polymer films of mass m_{dry} were incubated in DCM for 2 days. Samples were then extracted, dried under vacuum overnight and weighed as $m_{extracted}$. Gel content was calculated as:

$$X_G = \frac{m_{extracted}}{m_{dry}} \times 100\% \text{ (Equation 2)}$$

Contact angle

Advanced contact angle measurements were conducted with a Ram-Hart goniometer equipped with a microliter syringe. Measurements were taken on the most advanced side of the drop as the syringe tip was maintained inside of the ~5 µL drop. At least 6 measurements were taken across each film surface.

Thermal Characterization of SMP Films

Samples were sealed in aluminum pans and heated from -80°C to 150°C for two cycles on a TA Instruments (New Castle, DE) Q1000 differential scanning calorimeter (DSC). T_m and enthalpy change (ΔH_m) were recorded from the endothermic peak of the second cycle. Percent crystallinity ($\%X_C$) was calculated as the ratio of ΔH_m to 139.5 J/g, the ΔH_m^o for 100% crystalline PCL [100]:

$$\%X_C = \frac{\Delta H_m}{\Delta H_m^o} \times 100\% \text{ (Equation 3)}$$

Mechanical Characterization of SMP Films

To analyze the mechanical properties of the SMP films, two different tests were performed on a TA Instruments Q2000 dynamic mechanical analyzer (DMA). Rectangular strips (~20mm x ~3.0mm x ~0.3mm) were loaded onto a tension clamp. To determine storage modulus, $E_{st}'(37^oC)$, that is more reflective of response to strain over a particular area of the film, samples were subjected to a temperature sweep from 20°C to T_m +~15°C at a rate of 2°C/minute, a frequency of 1 Hz, and a constant strain of 0.2%. Maintaining this strain and frequency, samples were equilibrated at 5°C and held isothermally for 15 minutes. The storage modulus at 5°C, $E_{st}'(5^oC)$, was considered to be in the rubbery plateau region of all the copolymers, and as a result this information was used to derive the molecular weight between crosslinks, M_c [101, 102]. M_c was derived by first calculating the crosslinking density, ρ, expressed in moles of elastically effective network chains per mL, based on the kinetic theory of rubber elasticity and assuming that sample volumes do not change when subjected to small strains such that G' = E'/3 holds true :

$$\rho = \frac{E'(5^oC)}{3RT} \quad \text{(Equation 4)}$$

Then M_c was calculated by assuming all copolymers had a density equal to 10 kDa PCL at 25°C (1.146 g/mL according to Sigma-Aldrich), and dividing this density by ρ:

$$M_c = {}^{1.146}/_{\rho} \quad \text{(Equation 5)}$$

For determination of tensile modulus, $E_{tn}'(37^oC)$, in a manner more reflective of responses to stress across the entire film area, samples were equilibrated at 37 °C and subjected to a stress ramp of 0.1 MPa/min until break. Strain and stress at break, ε_{max} and σ_{max}, respectively, were also derived from this test.

***In vitro* degradation**

Polymer films of weight m_d were suspended in Gibco PBS and placed in a 37 °C, 5% CO2, 20% O_2 incubator for various time points. At each time point, the samples of each film were washed with distilled water, lyophilized, and weighed as m_e.

$$\%\text{Mass remaining} = \frac{m_e}{m_d} \times 100\% \quad \text{(Equation 6)}$$

Stress-Controlled Cyclic Thermomechanical Testing

Shape memory properties of cross-linked networks were characterized using the TA Instruments Q2000 DMA. Rectangular strips (~15mm x ~3.0mm x ~0.3mm) were loaded onto a tension clamp and subjected to three thermomechanical cycles consisting of the following four steps. The films were equilibrated at T_m+~15°C and subjected to tensile stress (0.004 MPa/min to 0.039 MPa) as shown in (1) of Figure 11. Films were then cooled (10°C/min to 0°C) (2), yielding the strain at the maximum stress $\varepsilon_1(N)$, before unloading the stress (0.004 MPa/min to 0 MPa) (3) and recording strain as $\varepsilon_u(N)$, the temporary shape. Finally, the films were heated (2°C/min to T_m+~15°C) (4) to recover the permanent shape $\varepsilon_p(N)$. The shape memory effect was quantified by shape fixity (R_f) and shape recovery (R_r). Shape fixity defines the ability to maintain a programmed shape induced by mechanical deformation,

while shape recovery describes how well shape is recovered (ε_p(N)) from the beginning of the N^{th} cycle (ε_p(N-1)):

$R_f(N) = \frac{\varepsilon_u(N)}{\varepsilon_1(N)} \times 100\%$ (Equation 7)

$R_r(N) = \frac{\varepsilon_1(N) - \varepsilon_p(N)}{\varepsilon_1(N) - \varepsilon_p(N-1)} \times 100\%$ (Equation 8)

Programming of SMP Shapes and Macroscopic Demonstration of Shape Memory Properties

Closed-end polymer tubes were prepared by first dipping a 0.90 mm outer diameter (O.D.) glass capillary with a thin layer of polyvinyl alcohol (PVA) and air drying for ~30 minutes. The PVA-coated capillary was then dipped in polymer solutions from the film preparation and UV-crosslinked (4.89 J/cm^2; 18.1 mW/cm^2). After solvent casting overnight, the tubes were placed under high vacuum for 30 minutes, immersed in deionized H_2O for 4 hours, and 100% ethanol for 2 hours. Films were then manually pulled off the glass capillary and washed in water for 2 hours to remove excess PVA. The tubes were dried overnight and the open side of the tube was closed by dipping it in polymer solution and UV crosslinking. Final dimensions of the tubes were approximately 1.0 – 2.0 cm in length, 0.90 mm in inner diameter, and 1.0 - 1.6 mm in O.D.

A guitar shape was prepared by first laser etching (Epilog Laser, Golden, CO) of a 2 mm PDMS mold containing a CAD-designed guitar. A 92%PCL-08%ACPCL polymer solution from the film preparation was then poured into the mold and UV crosslinked (26.1 J/cm^2; 290 mW/cm^2) on a 48^{o}C hotplate. The guitar was then placed under high vacuum for 30 seconds.

For macroscopic SM demonstration, closed-end tubes comprised of 88%PCL-12%ACPCL were heated in a 50^{o}C bath. The tubes were deformed with tweezers on each end and placed in an ice water bath for further deformation. Tweezers were removed from the tubes and the elongated thread-like or corkscrew temporary shape was set at room temperature for measurement. The original tube dimensionality was recovered by placing in a 37^{o}C water bath. Guitars comprised of 92%PCL-08%ACPCL were recovered at 47 ^{o}C in a water bath.

Cell viability studies

Polymer disks with ~50 µm thickness and 14.3 mm in diameter were leached in ethanol for approximately 48 hours to remove remaining DMPA photoinitiator. Films were then washed twice for several hours with MesoEndo Endothelial Cell Growth Media (Cell Applications, Inc. San Diego, CA) and incubated at 37^{o}C.

Cell viability was measured in two different settings. The first setting was to determine cytotoxicity of leachables from test films. For this condition, 15,000 passage 9 (P9) red fluorescent protein-expressing human umbilical vascular endothelial cells (RFP-HUVECs, Angio-Proteomie, Boston, MA) were seeded on TCPS in a 96-well plate, and after 1.5 hours at 37^{o}C polymer half-disks were submerged in 150 µL MesoEndo media. The second setting was to compare the viability of the cells seeded exclusively on either the polymer film surfaces or TCPS (Control). To prevent cell attachment on TCPS underneath test polymer films, wells were coated with a 1% agarose solution. The agarose-coated wells were dried, washed with 100% ethanol twice for 1 hour each, UV sterilized for 1 hour, and washed twice with MesoEndo media for 1 hour each at 37^{o}C. Media-soaked polymer disks were then placed on the agarose-coated wells, and RFP-HUVECs (15,000/polymer) were seeded directly on the film surfaces.

After 1.5 hours, 150 µL of media were added. RFP-HUVECs (15,000/well) seeded on TCPS and 1% agarose-coated TCPS were used as positive and negative controls, respectively. A standard curve was generated from TCPS wells seeded with 11,250, 7,500, and 3,750 RFP-HUVECs.

For the above experiment, viability was assessed at 9 hour, 35 hour, and 91 hour time points via the resazurin assay [103]. Briefly, 150 µL of resazurin sodium salt (Sigma-Aldrich) at the final concentration of 5 µM in MesoEndo media was added to each well. After 4 hour incubation at 37^{o}C, 100 µL from each well was transferred to a new 96-well plate and 560/590 nm excitation/emission was read on an Infinite® M1000 Pro plate reader (Tecan Group Ltd, San Jose, CA). Fluorescence signals were adjusted for baseline readings from any autofluorescence under different conditions without cells (e.g. each polymer film in TCPS and 1% agarose-coated TCPS). Viable cell number was calculated based on a standard curve from TCPS standards, and % Cell viability was normalized to fluorescence readings of TCPS controls seeded with 15,000 cells. All samples were tested in quadruplicates.

In another experiment to investigate the cell morphology on the polymer disks, P5 human coronary artery endothelial cells (hCAECs) (Cell Applications, Inc., San Diego, CA) were seeded directly onto polymer disks, similar to the above. After 3 days of incubation on the disks or TCPS, cells were fixed with 4% paraformaldehyde for 15 min, permeabilized with 0.5% Triton X-100 for 10 min, and blocked with 10% Bovine Serum Albumin for 30 minutes. Cells were then incubated with 2 µM Ethidium Homodimer-1 for 10 min and 50 µM Alexa Fluor® 488 Phalloidin (Molecular Probes, Eugene, OR) for 20 min. Cells on polymer surfaces were imaged on a LSM 510 META Inverted Confocal Microscope (Carl Zeiss, LLC, Thormwood, NY), while TCPS controls were imaged with a Nikon Eclipse Ti inverted fluorescence microscope (Nikon Instruments Inc. Melville, NY). Images were postprocessed and analyzed using ImageJ software (NIH, Bethesda, MD).

***In vivo* external vascular bypass graft**

A proof-of-concept study was performed to demonstrate the utility of these materials for external vascular treatment of occluded blood vessels in a rat double carotid artery ligation model (Figure3). All rat surgical procedures were approved by the Institutional Animal Care and Use Committee (IA-CUC) at Vanderbilt University. Immediately prior to surgery, closed-end SMP tubes (1.5 cm in length, 1.2 cm O.D.) comprised of 89%PCL-11%ACPCL were UV sterilized and collagen gels containing pro-angiogenic C16 and anti-inflammatory Ac-SDKP peptides were prepared as described previously [91]. Briefly, 700uL PureCol® 3 mg/mL Bovine Collagen Solution (Advanced BioMatrix, Inc. San Diego, CA) containing 75 µg of both C16 and Ac-SDKP peptides was adjusted to pH 8 with 0.1 N NaOH and incubated at 37^{o}C for 30 minutes to form a gel.

Rats were subjected to a double ligature and complete transection of the right common carotid artery. One untreated control rat died unexpectantly three days after surgery. Test groups (n = 2-3) were SMP tube grafting with treatment of collagen gel containing C16 and Ac-SDKP (“Polymer + Peptides”), treatment of only collagen gel containing C16 and Ac-SDKP (“Peptide Only”), and untreated (negative control). In the polymer + peptides group (n=3), SMP tubes were implanted immediately following the ligations. By positioning the start and end of the tube beyond the location of both ligatures, the tube completely covered the occluded area. Each tube end was then tied to the native artery by suturing. The SMP tube and the adjacent occluded region of the carotid artery were then embedded in the collagen gel containing peptides by cotton swab application. The collagen gel was applied immediately following the ligations in the Peptide Only group (n=2) in the same manner. All incisions were sutured closed using non-degradable sutures. Rats were given buprenorphine 0.05 mg/kg SQ every 8-12 hours as needed for pain and monitored for two weeks.

Following the two week implantation, fluorescence microangiography was performed to assess capillary growth from the occluded vessel and verify if blood perfusion occurred through the tube [91]. The inferior vena cava of each rat was cut and the vasculature was flushed by injecting heparinized saline followed by injection of 0.1 µm diameter FluoSpheres® Carboxylate-Modified Red Fluorescent Microspheres (Life Technologies Corp., Carlsbad, CA) in heparinized saline (1:20 dilution) through the left ventricle. In this manner, the beads perfuse through all functional vessels in the body, including those formed in and around the polymer tubes. Perfusion of the beads through the polymer tube and native artery were then observed using a LSM 510 META Inverted Confocal Microscope (Carl Zeiss, LLC) under both fluorescent and brightfield modes.

To visualize tissue morphology and identify cellular composition around the polymer and native artery, hematoxylin and eosin (H&E) and immunofluorescent (IF) staining, respectively, were performed. Tissue containing the polymer tube and native artery were embedded in optical cutting temperature (OCT), frozen at -80℃ for 24 hours, and sectioned (5 µm sections) using a cryotome. For IF staining, frozen sections were stained with mouse anti-rat phycoerythrin (PE)-conjugated CD31 (clone TLD-3A12, BD Biosciences) as an endothelial cell marker and mouse anti-rat FITC-conjugated CD45 (OX-1, BD Biosciences) as a leukocyte marker, then counter-stained with Hoechst 33258 nuclear stain (Life Technologies, Inc.). The Nikon Eclipse Ti inverted fluorescence microscope was used to capture images of OCT sections for H&E and IF staining.

Statistical Analysis

All data are reported as means ± standard error of the mean (SEM). In comparisons between individual groups, an unpaired, two-tailed Student's t-test was used and $p < 0.05$ was considered statistically significant.

Principal component analysis (PCA) was used to determine correlations between material properties by comparing the means of the corresponding variables for each polymer composition. PCA reduces the variable space down to a set of components. An $n \times p$ matrix was comprised that contained the mean values of each variable to be compared, p, for each polymer composition, n. The variables of the matrix were standardized to their z-score for more apt comparison between variables, and the covariance matrix was computed. Plots of the covariance matrix were generated. All analysis was done with MATLAB (Mathsoft, Natick, MA) using the program written in Appendix Q.

Results

Synthesis and characterization of α-allyl carboxylate-ε-caprolactone (ACCL) monomer

Synthesis of the novel ACCL compound was achieved by carbanion activation of ϵ-caprolactone and subsequent reaction with allyl chloroformate (Figure 1). The ^{1}H-NMR spectra is shown in Appendix B. The additional peak present at 2.65 ppm corresponds to the two α-protons in ϵ-caprolactone and indicates that the purity of the ACCL product is approximately 98% after column chromatography, with 2% ϵ-caprolactone impurity. This purity was deemed acceptable for copolymerization.

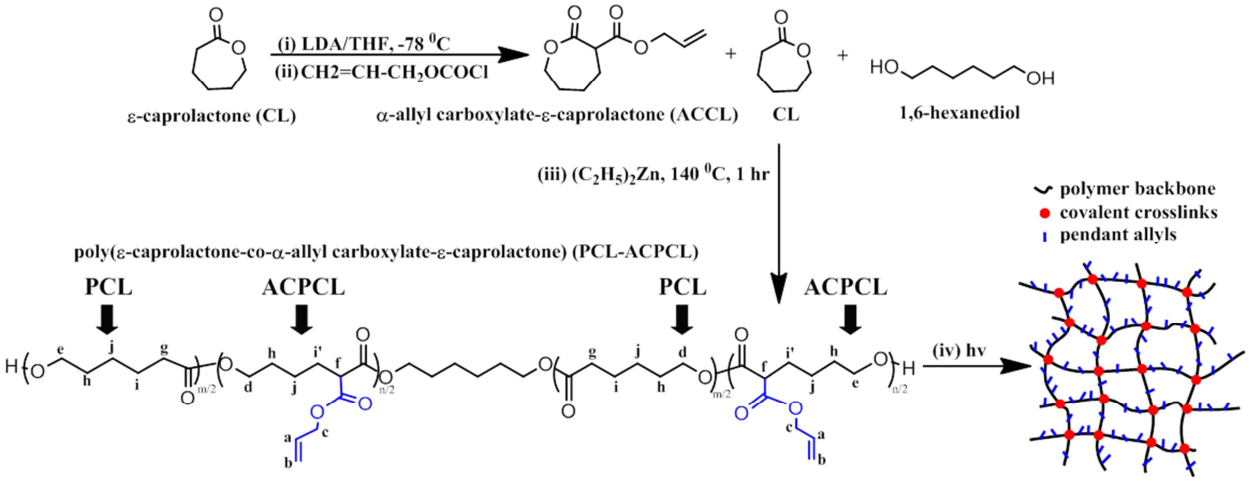

Figure 4: Synthesis of ACCL monomer and x%PCL-y%ACPCL copolymers. ACCL monomer is synthesized by carbanion activation and reaction with allyl chloroformate. Ring-opening polymerization of ACCL with CL forms the final random x%PCL-y%ACPCL copolymers, where x and y represent the respective molar ratios of each unit. Shape memory polymers (SMPs) were made from these copolymers by UV irradiation, which allowed formation of covalent bonds between polymer chains via the pendant allyl groups.

Synthesis and characterization of polymers

As shown in Figure 4, novel x%PCL-y%ACPCL copolymers were synthesized by ring-opening polymerization (ROP) of ACCL and ϵ-caprolactone (CL) using a 1,6-hexanediol initiator and a diethylzinc catalyst that had proven effective in copolymerizing a different allyl ester-based monomer [104]. The highly reactive diethylzinc catalyst resulted in almost immediate polymerization, as evidenced by abrupt viscosity changes. Some observable inter-chain cross-linking occurred immediately upon diethylzinc injection that reduced overall yields between 21.7 and 70.7% (Table 1). Inconsistencies in polydispersity (PDI), molecular weight, and yields relate in large part to how well-distributed this catalyst was in solution. In support of this claim, 92%PCL-08%ACPCL had the best distribution of catalyst in solution as it was the only solution where the diethylzinc-containing syringe was dispensed while submerged in the monomer solution instead of on top of it, and resulted in the lowest PDI (1.59) and highest yield (70.7%). Future copolymers will be catalyzed in this manner to attain lower PDIs, more consistent molecular weights, and higher yields.

Polymer composition can be finely tuned by controlling ACCL:CL monomer feed ratios. There was a good linear correlation (Appendix C: R^2 = 0.957) between monomer feed ratio and x and y% polymer composition for the 8 compositions synthesized (Table 1). Molar composition, which was determined by ^{1}H-NMR (Appendix D), ranged from y = 4.16 - 17.86%. The consistency and color of each copolymer was reflective of its molar composition and molecular weight distribution, as shown in Appendices E and F. The majority of copolymers had a powder consistency, but the two copolymers with the highest M_w (y = 11.2% and 5.74%) were powders intermixed with clear transparent film fragments, and the lowest molecular weight copolymer, y = 17.86%, was a slurry at room temperature and was excluded from most analyses. In general, increasing y%ACPCL and PDI increased the amount of red-orange color in the copolymer.

Number-average molecular weight (M_n) was controlled by the 1,6-hexanediol initiator: total monomer ratio, although there were some exceptions. The copolymer with the highest y%ACPCL,

82%PCL-18%ACPCL, was of markedly lower M_n (8.4 kDa) than the rest of the copolymers with the same initiator: monomer ratio, suggesting that higher y%ACPCL compositions are more difficult to polymerize. Besides this one outlier, a 1:200 1,6-hexanediol initiator: total monomer ratio produced fairly consistent M_n's (12.1 – 16.5 kDa), which was comparable to the 100%PCL-dimethacrylate control (Appendix G: 11.6 kDa). Further increasing this ratio beyond 1:200 resulted in higher molecular weight polymers (M_n = 19.1 – 29.7 kDa) as expected. However, a 1:250 ratio resulted in a higher molecular weight polymer than both 1:315 and 1:330 ratios, indicating a difficulty in controlling molecular weight. Again, better distribution of catalyst in solution will likely result in tighter control of copolymer molecular weight via the initiator: total monomer ratio.

Table 1: Synthesis Table of x%PCL-y%ACPCL Copolymers

Copolymer	y%ACPCL		Yield [%]	Initiator: Monomer	M_n [Da]	M_w [Da]	PDI
	Theoretical y [%]	Actual y [%]					
96%PCL-04%ACPCL	8.2	4.16	44.8	1:200	15060	26870	1.78
94%PCL-06%ACPCL	9.0	5.74	38.3	1:200	16546	39050	2.36
92%PCL-08%ACPCL	14.2	8.04	70.7	1:330	22026	35074	1.59
89.4%PCL-10.6%ACPCL	16.2	10.58	39.8	1:200	13627	34049	2.50
89%PCL-11%ACPCL	16.8	11.20	21.7	1:250	29709	48842	1.64
88%PCL-12%ACPCL	17.2	11.66	22.6	1:315	19087	36430	1.91
85%PCL-15%ACPCL	22.5	14.50	56.6	1:200	12095	28931	2.39
82%PCL-18%ACPCL	31.5	17.86	47.7	1:200	8375	19987	2.39

Thermal characterization of polymers prior to crosslinking

Melting temperatures (T_m's) of the x%PCL-y%ACPCL polymer library before crosslinking ranged from 48.0^{o}C for 92%PCL-08%ACPCL to 32.5^{o}C for 85%PCL-15%ACPCL (Table 2). The 82%PCL-18%ACPCL copolymer had a melting temperature of ~25.2^{o}C but was excluded from this table because this melting temperature was determined to be too low for useful biomedical application. A cursory look at thermal properties (T_m, ΔH_m, T_c, ΔH_c, and X_C) for the uncrosslinked x%PCL-y%ACPCL polymer library in Table 2 suggests that these thermal properties are dependent on molar composition, but also seem to be affected by other factors such as molecular weight characteristics (M_n, M_w, and PDI). A plot Principle component analysis (PCA) was utilized to determine how these thermal properties correlate with x%PCL and molecular weight characteristics for the 7 different polymers synthesized (y = 17.86% copolymer excluded) and a 100%PCL control (M_n = 11.3 kDa – see Appendix G). As thermal properties are influenced by physiochemical characteristics (molar composition and size), analysis focused on the correlations between physicochemical characteristics (independent variables) and thermal properties (dependent variables) of polymers. The results revealed that thermal properties are heavily dependent on molar composition (x% and y%) but also are influenced by the molecular weight characteristics of the polymer. All the test polymers had a stronger dependence on x%PCL than any of the molecular weight properties, but M_w and PDI still had a strong influence. The dependence of thermal properties on x%PCL ranked from $T_c > \Delta H_m \sim \Delta H_c > T_m$ prior to crosslinking, implying that T_m is least affected by molar composition in the uncrosslinked state. PCA served as a useful tool in demonstrating a strong dependence of thermal properties on molar composition and, to a lesser extent, molecular weight characteristics.

Table 2: Thermal Properties of x%PCL-y%ACPCL library

Composition	T_m [^oC]	ΔH_m [J/g]	X_C [%]	T_C [^oC]	ΔH_C [J/g]	T_g [^oC]
100%PCL	53.0 ± 0.2	79.0 ± 2.1	56.6 ± 1.5	32.7 ± 0.2	78.7 ± 2.3	-60.4 ± 4.7
100%PCL-DMA	50.7 ± 0.5	63.8 ± 2.9	45.8 ± 1.9	27.7 ± 0.2	64.5 ± 3.4	-58.6 ± 2.9
96%PCL-04%ACPCL	45.9 ± 0.3	58.1 ± 1.7	41.6 ± 1.2	23.2 ± 0.3	59.5 ± 1.2	-59.9 ± 3.1
94%PCL-06%ACPCL	47.1 ± 0.1	50.3 ± 0.7	36.1 ± 0.5	11.1 ± 0.2	50.0 ± 0.8	-60.3 ± 2.9
92%PCL-08%ACPCL	48.0 ± 0.3	48.8 ± 1.5	35.0 ± 1.1	13.3 ± 1.2	50.7 ± 1.2	-62.7 ± 0.7
89.4%PCL-10.6%ACPCL	39.1 ± 0.3	42.3 ± 1.0	30.4 ± 0.7	-1.6 ± 0.4	42.1 ± 0.6	-62.8 ± 1.2
89%PCL-11%ACPCL	42.9 ± 0.3	39.2 ± 1.3	28.1 ± 1.0	3.0 ± 0.8	40.3 ± 1.2	-61.3 ± 1.4
88%PCL-12%ACPCL	41.6 ± 0.2	43.3 ± 1.0	31.1 ± 0.7	-0.3 ± 0.1	43.6 ± 1.2	-63.8 ± 0.9
85%PCL-15%ACPCL	32.5 ± 0.4	34.0 ± 1.2	24.4 ± 0.9	-9.5 ± 4.2	33.5 ± 2.5	-61.8 ± 2.0

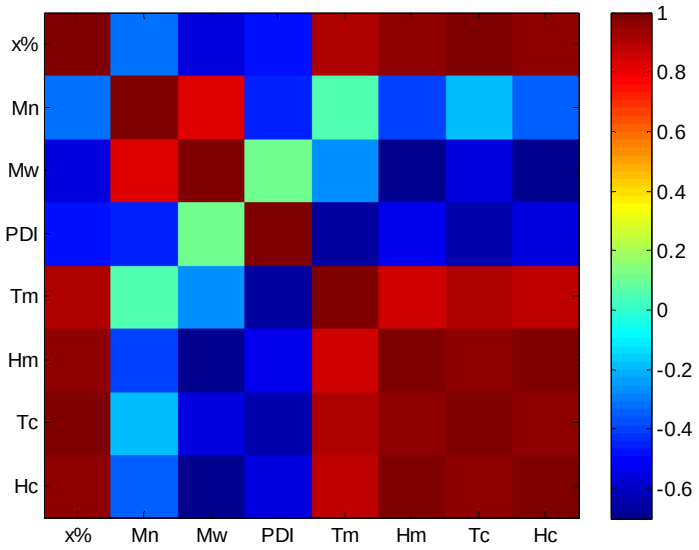

Figure 5: Heat map of PCA analysis demonstrating degree of covariance between chemical, physical, and thermal properties for copolymer library prior to crosslinking. The degree of covariance between properties is indicated by the color map, indicating the nature (positive or negative) and degree (darkness) of correlation between the variables. For instance, dark red indicates a strong positive correlation (up to 1.0) and dark blue indicates a strong negative correlation (up to 0.64). T_m is most influenced by x%PCL (dark red – directly proportional) and PDI (dark blue – inversely proportional), and correlates well (red) with the other thermal properties as expected.

Gel content, crosslinking density, and thermal characterization of SMP Films

Gel content, crosslinking density, thermal, mechanical, contact angle, shape memory, and degradation properies of test films were assessed. Table 3 tabulates values of gel content (X_G), crosslinking density (ρ), molecular weight between crosslinks (M_c), and thermal properties. Gel content (X_G), which relates to the percent crosslinking of the material, was an average of 60.5 ± 12.5% for all the test films. Crosslinking density, ρ, expressed in moles of elastically effective network chains per mL, and molecular between crosslinks, M_c, are important structural parameters for crosslinked networks derived from the rubber elasticity theory [105], and are inversely related to each other by equation 5. As with the uncrosslinked copolymers, there once again appears to be a strong dependence of thermal properties on

molar composition (Figure 5, Table 3, and Appendix I). For SMP films of y = 0 – 14.50%, values of ρ and M_c range from 49.2 – 3.7 mmoles/mL and 23 – 300 Da, respectively. T_m of x%PCL-y%ACPCL SMP films range from 45.4 – 28.6°C. Enthalpy of fusion, ΔH_m, ranged from 51 – 20 MPa with percent crystallinity, X_c, correspondingly between 37 –14% in comparison. Crystallization temperatures decreased from 18.6 °C to -14.0 °C as y%ACPCL increased from 4.16 to 14.50%. The overlay in Figure 5 illustrates this clear downward shift in T_m and ΔH_m as x%PCL is decreased in the copolymers. A plot of thermal properties versus y%ACPCL for films with X_G close to 60% (Appendix I) follows an approximately linear decrease with increasing y%ACPCL. However, these trends are not independent of other variables such as molecular weight characterisitics, X_G, ρ, and M_c.

Table 3: Gel content, crosslinking density and Thermal properties of x%PCL-y%ACPCL SMP Films

Composition	X_G [%][1]	ρ [mmole /mL][1]	M_c [Da][1]	T_m [°C]	ΔH_m [J/g]	X_C [%]	T_C [°C]	ΔH_C [J/g]	T_g [°C]
100%PCL-DMA	72.0 ± 17.3	49.2	23.3	48.1 ± 0.4	48.2 ± 0.5	34.6 ± 0.4	19.5 ± 1.0	48.6 ± 0.4	-54.2 ± 3.0
96%PCL-04%ACPCL	36.7 ± 8.6	30.2	37.9	45.4 ± 0.2	50.9 ± 2.0	36.5 ± 1.4	18.6 ± 1.3	50.2 ± 1.1	-59.4 ± 0.1
	63.0 ± 8.6	30.7	37.3	43.4 ± 1.2	44.6 ± 3.2	32.0 ± 2.3	15.8 ± 0.9	43.2 ± 6.1	-56.9 ± 0.1
94%PCL-06%ACPCL	60.3 ± 21.3	17.3	66.2	37.9 ± 0.9	39.1 ± 5.3	28.0 ± 3.8	2.4 ± 0.5	38.7 ± 4.8	-58.8 ± 4.9
92%PCL-08%ACPCL	73.2 ± 12.0	15.3	74.9	39.0 ± 0.3	35.3 ± 1.8	25.3 ± 1.3	5.3 ± 0.8	35.3 ± 1.8	-59.2 ± 1.5
89.4%PCL-10.6%ACPCL	49.0 ± 6.2	18.2	62.9	37.9 ± 0.7	38.7 ± 1.6	27.7 ± 1.2	-2.1 ± 0.7	36.5 ± 0.8	-57.1 ± 1.5
	78.2 ± 0.6	3.5	323.6	27.5 ± 3.0	19.7 ± 6.7	14.1 ± 4.8	-10.0 ± 5.2	11.9 ± 8.2	-57.5 ± 0.3
89%PCL-11%ACPCL	71.2 ± 6.7	7.4	155.4	35.1 ± 0.5	31.2 ± 1.1	22.4 ± 0.8	-6.1 ± 0.8	32.6 ± 0.8	-58.0 ± 3.7
88%PCL-12%ACPCL	64.1 ± 3.1	16.6	69.0	33.4 ± 1.2	33.7 ± 1.1	24.2 ± 0.8	-8.7 ± 0.2	31.4 ± 2.2	-58.7 ± 2.2
85%PCL-15%ACPCL	50.3 ± 0.6	3.8	300.5	29.7 ± 0.2	28.3 ± 2.7	20.3 ± 1.9	-13.9 ± 0.8	17.2 ± 0.9	-57.5 ± 1.1
	72.7 ± 2.5	3.7	309.7	28.6 ± 0.2	22.1 ± 0.9	15.8 ± 0.7	-14.0 ± 0.3	13.1 ± 0.8	-57.3 ± 1.5

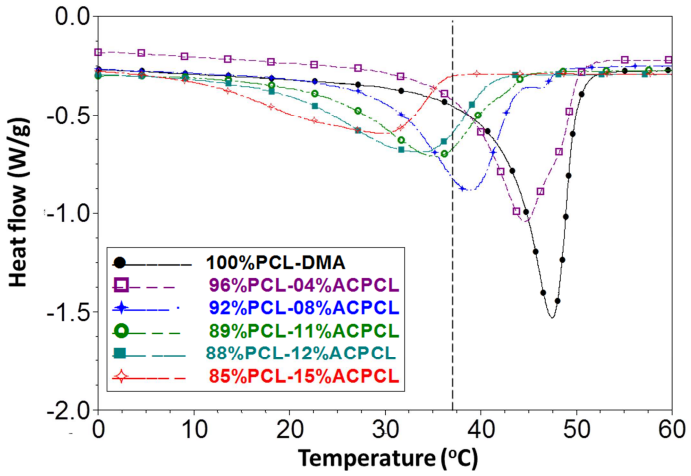

Figure 6: Overlay of Thermal Properties for SMPs. Differential Scanning Calorimetry (DSC) plots of copolymer and 100%PCL-dimethacrylate select films demonstrate a clear dependence of T_m, ΔH_m, and $\%X_C$ on y%ACPCL. As y%ACPCL increases, values of these properties decrease.

PCA enables independent evaluation of variable correlations with thermal properties. As shown in Figure 7, thermal properties had the strongest correlation with ρ, x%PCL, and PDI. Interestingly, all thermal properties except for T_c had a greater correlation with ρ (rho) than with x%PCL. Of the molecular

weight parameters, thermal properties correlated most inversely with PDI. Examination of ρ correlations with independent variables reveals that ρ correlates strongest with x%PCL and M_w. These analytic results suggest that PDI and ρ independently contribute to thermal properties, in addition to x%PCL. The enthalpies ΔH_m and ΔH_c were also correlated with variable X_G, indicating that gel content can be tuned to control enthalpies without as much of an effect on transition temperatures T_m and T_c. Correlation of thermal properties with independent variables are as follows: T_m (ρ > x%PCL > PDI >> M_w > X_G), T_c (x%PCL > ρ > PDI > M_w >> X_G), ΔH_m (ρ > x%PCL > X_G > PDI > M_w), and ΔH_c (ρ ~ x%PCL > PDI > X_G >> M_w). In summary, ρ is influenced most by molar composition and M_w, and it has the greatest correlation with most thermal properties. Molar composition and PDI also appear to independently effect thermal properties.

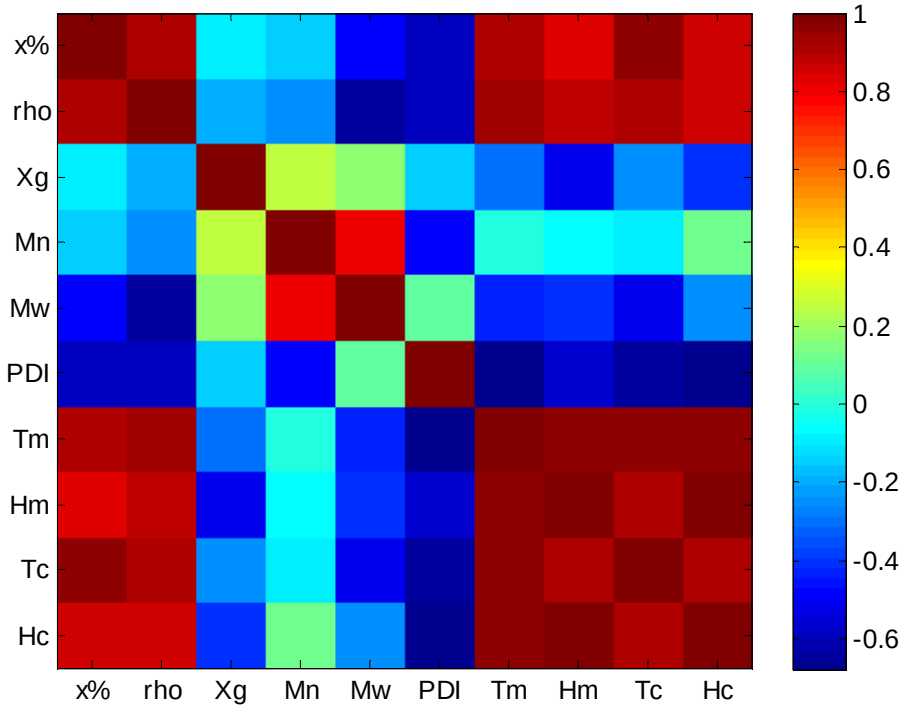

Figure 7: Heat map of PCA analysis demonstrating degree of covariance between chemical, physical, and thermal properties for SMP films. The degree of covariance between properties is indicated by the color map, indicating the nature (positive or negative) and degree (darkness) of correlation between the variables. For instance, dark red indicates a strong positive correlation (up to 1.0) and dark blue indicates a strong negative correlation (down to -0.65). Thermal properties correlate strongest with ρ (dark red), x%PCL (dark red) and PDI (dark blue).

Mechanical characterization of SMP Films

Mechanical properties of the films were also assessed for the SMP library and are reported in Table 4. Moduli were comparable for 100%PCL-DMA and 96%PCL-04%ACPCL, but in a similar manner to thermal properties, decrease with increasing y%ACPCL (Figure 8). Tensile modulus at 37°C, E_{tn}'(37°C), ranged from 75.9 for 96%PCL-04%ACPCL to 2.2 MPa for 85%PCL-15%ACPCL. Strain to break, ε_{max}, was a highly variable quantity but was >100% on average for most compositions. For all test films except those with the highest allyl content (i.e. 85%PCL-15%ACPCL), maximum stress, σ_{max}, was between 1.0 – 3.3 MPa. The σ_{max} of 85%PCL-15%ACPCL test films was much lower, at < 0.4 MPa.

To examine relationships between variables, PCA was again conducted with physiochemical, thermal, and mechanical properties ($E_{st}'(37^oC)$, $E_{tn}'(37^oC)$, ε_{max}, and σ_{max}). As indicated in Figure 9, $E_{st}'(37^oC)$ and $E_{tn}'(37^oC)$ correlate strongest with ρ > x%PCL > M_w > PDI. Crosslinking density ρ, which correlated with x%PCL and M_w itself, appears to be the most important parameter for these properties. The correlations of $E_{st}'(37^oC)$ and $E_{tn}'(37^oC)$ are most similar to those of T_m and T_c, with the one difference that M_w is more influential than PDI on these mechanical properties. The σ_{max} correlates strongest with x%PCL > ρ > PDI > M_w from most to least. These dependencies are most similar to $E_{st}'(37^oC)$, so it appears that these two parameters are governed by very similar principles. On the other hand, strain to break, ε_{max}, did not correlate well with the other mechanical properties. The ε_{max} had the strongest correlation to M_n and M_w of any of the variables examined and was relatively independent of x%PCL, PDI, and ρ. It therefore may be an effective strategy to increase ε_{max} by increasing M_n, as no other parameters had a strong correlation with this variable. One possible explanation for this correlation may be that higher molecular weight polymers undergo more chain entanglements and are less susceptible to rupture. It is also possible, however, that this is the result of the inherent variability of the measurement itself. Nonetheless, from this analysis it appears that increasing M_n may lead to more ductile materials without affecting other material properties.

Table 4: Mechanical properties of SMP films

Composition	X_G [%]	M_c [Da]	T_m [^oC]	$E_{st}'37^oC$ [MPa][1]	$E_{tn}'37^oC$ [MPa][2]	ε_{max} [%]	σ_{max} [Mpa]
100%PCL-DMA	61.7 ± 1.8	23.3	46.4 ± 2.6	136.8 ± 46.2	53.8 ± 36.7	199.5 ± 71.2	4.68 ± 0.3
96%PCL-04%ACPCL	36.7 ± 8.6	37.9	45.4 ± 0.2	130.0 ± 49.3	75.9 ± 32.9	39.8 ± 55.9	1.81 ± 1.0
	63.0 ± 8.6	37.3	43.4 ± 1.2	186.1 ± 3.1	55.0 ± 17.1	93.4 ±135.5	3.3 ± 0.4
94%PCL-06%ACPCL	60.3 ± 21.3	66.2	37.9 ± 0.9	103.4 ± 5.0	3.05 ± 2.6	253.0 ±19.4	2.36 ± 0.9
92%PCL-08%ACPCL	73.2 ± 12.0	74.9	39.0 ± 0.3	74.4 ± 42.5	18.6 ± 9.9	353.4 ± 50.6	2.46 ± 0.02
89.4%PCL-10.6%ACPCL	49.0 ± 6.2	62.9	37.9 ± 0.7	75.7 ± 24.8	4.53 ± 3.4	131.4 ± 81.9	0.77 ± 0.6
	78.2 ± 0.6	323.6	27.5 ± 3.0	24.7 ± 6.2	3.08 ± 2.6	101.0 ± 68.4	0.68 ± 0.2
89%PCL-11%ACPCL	71.2 ± 6.7	155.4	35.1 ± 0.5	45.6 ± 15.2	5.44 ± 1.1	300.2 ± 126.7	1.14 ± 0.3
88%PCL-12%ACPCL	64.1 ± 3.1	69.0	33.4 ± 1.2	67.8 ± 27.0	4.24 ± 1.1	84.5 ± 89.1	0.99 ± 0.6
85%PCL-15%ACPCL	50.3 ± 0.6	300.5	29.7 ± 0.2	16.4 ± 0.6	2.18 ± 0.1	28.1 ± 32.2	0.12 ± 0.1
	72.7 ± 2.5	309.7	28.6 ± 0.2	16.1 ± 6.3	3.11 ± 0.4	82.8 ± 48.6	0.36 ± 0.1

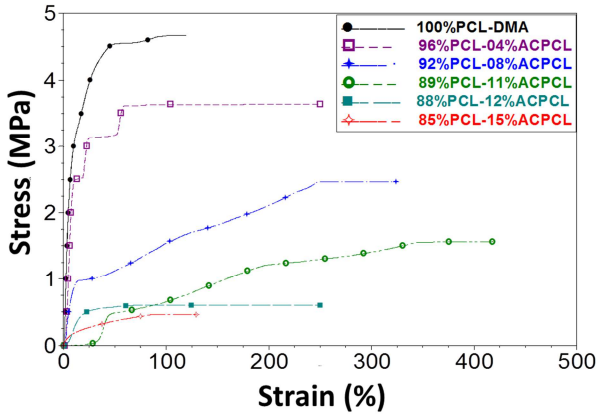

Figure 8: Overlay of Mechanical Properties for SMPs. A dynamic mechanical analyzer (DMA) was used to conduct a tensile test of the films under a stress ramp of 0.1 MPa/min until break. Tensile modulus, $E_{tn}'(37^oC)$, was calculated based on the slope of stress vs. strain curves. Similar to thermal properties, as y%ACPCL increases, modulus tends to decrease.

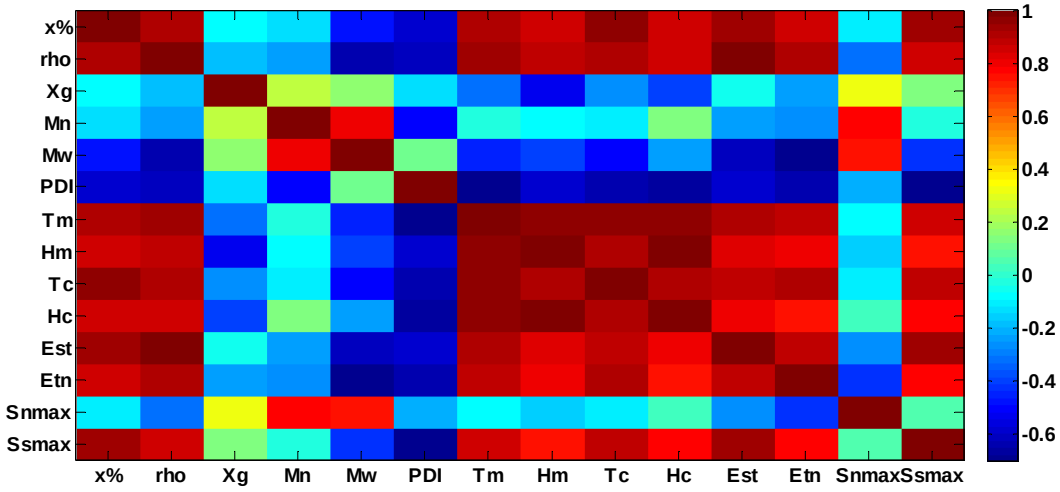

Figure 9: Heat map of PCA analysis demonstrating degree of covariance between chemical, physical, thermal, and mechanical properties for SMP films. The degree of covariance between properties is indicated by the color map, indicating the nature (positive or negative) and degree (darkness) of correlation between the variables. For instance, dark red indicates a strong positive correlation (up to 1.0) and dark blue indicates a strong negative correlation (up to 0.65). $E_{st}'(37^oC)$ and $E_{tn}'(37^oC)$ correlate strongest with ρ, x%PCL, M_w, and PDI in that order. From most to least, ε_{max} correlates with M_n, M_w, and ρ, while σ_{max} correlates strongest with x%PCL, ρ, PDI, and M_w.

Contact angle characterization of SMP Films

Advanced contact angle measurements, θ_{adv}, were taken on test film surfaces using water to determine relative hydrophobicity of the films. Films were relatively hydrophobic, with values ranging from 70^o – 83.5^o (Appendix J). There were statistically significant differences in contact angle between 100%PCL-DMA films (76.5 ± 7.8^o) and 94%PCL-06%ACPCL (80.0 ± 7.8^o), 92%PCL-08%ACPCL (79.5 ± 5.1^o), 89%PCL-11%ACPCL (70.5 ± 1.7^o), and 85%PCL-15%ACPCL (83.5 ± 7.1^o).

Shape memory properties of SMP Films

Shape memory properties of the x%PCL-y%ACPCL crosslinked networks were quantified by thermomechanical cycling and tested in macroscopic demonstrations. For shape memory quantification, shape fixity (R_f) and recovery (R_r) were determined by thermomechanical cycling, as depicted in Figure 10. Films were heated and (1) programmed into an elongated shape by subjecting to tensile stress, (2) cooled to yield the strain at the maximum stress $\varepsilon_1(N)$, (3) unloaded of stress to generate temporary shape $\varepsilon_u(N)$, and (4) heated to recover permanent shape $\varepsilon_p(N)$. Select films of every composition exhibited $R_f > 98\%$, and all but 89%PCL-11%ACPCL and 85%PCL-15%ACPCL test films exhibited shape recovery after the first cycle $R_r(N) \geq 98\%$ (Table 5). These same two films had far lower shape recovery after the first cycle, $R_r(1)$, (< 65%) than the other test films (> 86%). The maximum strain, $\varepsilon_1(N)$, from 0.039 MPa applied stress was highly variable, ranging from 6 – 122% in this cycling procedure.

PCA was conducted on four shape memory properties ($R_r(1)$, $R_r(N)$, $R_f(N)$, and $\varepsilon_1(N)$) with all parameters as before in order to better understand the fundamental principles responsible for the trends in shape memory properties. $R_r(N)$ appeared to correlate most with y%ACPCL and was not influenced as much by any other physiochemical parameters (Figure 11). Interestingly, out of all the thermal and mechanical properties, it correlates strongest with $T_{c,}$ which implies that the fixing temperature was not low enough for the high y%ACPCL copolymers to attain better shape recovery. Indeed, it was demonstrated in previous studies that greater shape recovery is achieved when polymers are fixed at or below their crystallization temperature [106, 107]. Shape recovery from the first cycle, $R_r(1)$, was accounted for merely to demonstrate that repeated cycling can improve shape recovery. It correlated strongest with $R_r(N)$ and was most affected by independent variable ρ (rho). Meanwhile, both $R_f(N)$ and the strain attained from fixing at 0.039 MPa, $\varepsilon_1(N)$, correlated strongest with X_G. In particular, $R_f(N)$ does not appear to correlate strongly with any other variables, suggesting that X_G may be the sole driving force for this parameter. Therefore, shape memory properties may be further improved by adjusting gel content and lowering fixing temperatures below T_c in the programming step. Other programming parameters such as deformation temperature and stress or strain rate could also be adjusted to improve shape memory properties. Notably, Table 2 shows that films with the highest $\varepsilon_1(N)$ had very good shape fixity and recovery, intimating that strain rate could potentially be a more effective programming strategy. Although further improvements are possible, films of all compositions, with perhaps the exception of 85%PCL-15%ACPCL, possess good shape memory characteristics.

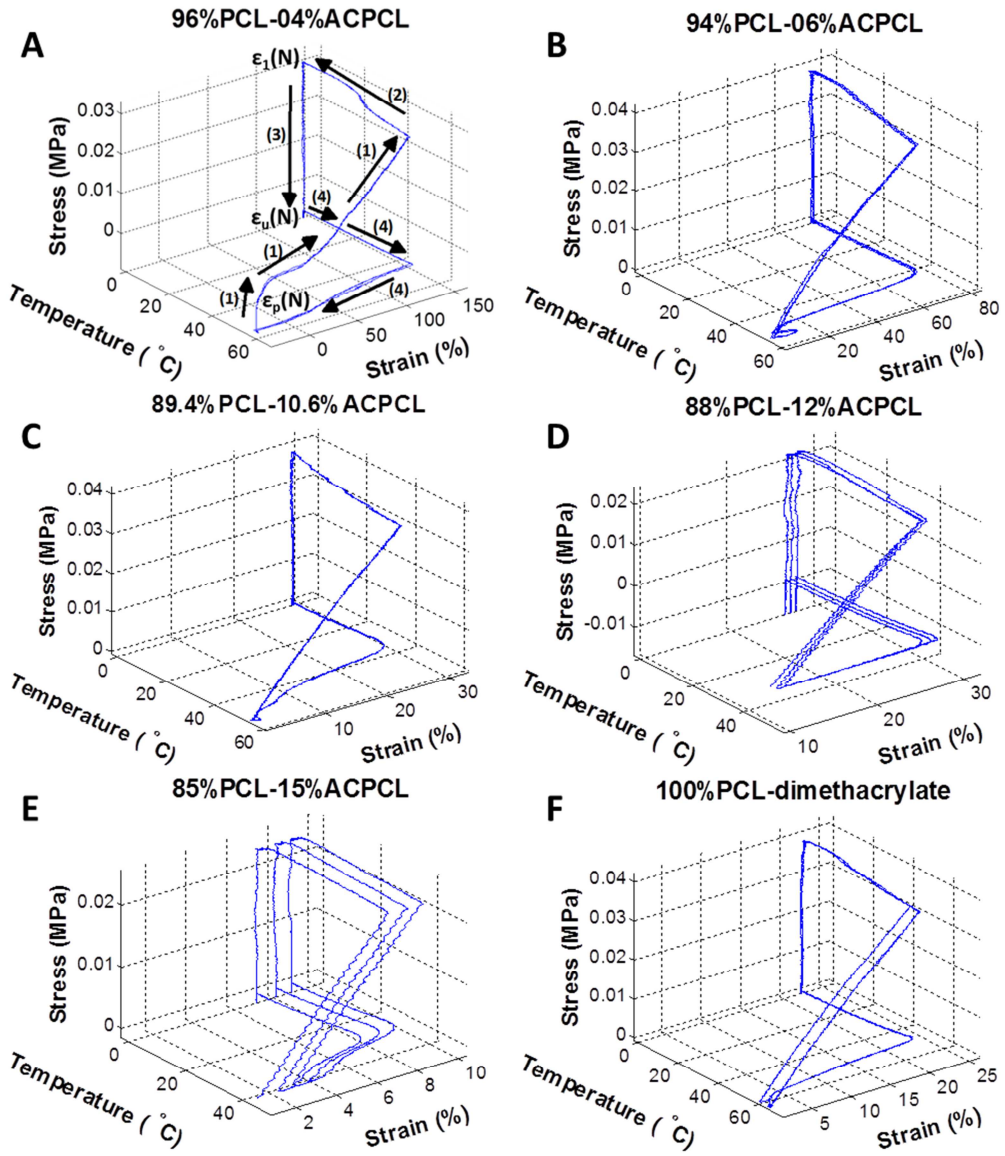

Figure 10: Stress-Controlled Thermomechanical Cycling of SMPs. SMP films were heated to T_m+~15°C and (1) programmed into an elongated shape by subjecting to tensile stress (0.004 MPa/min to either 0.039 MPa (or 0.023 MPa for E) and cooled (10°C/min to 0°C) (2) yielding the strain at the maximum stress ε_1(N). Stress was then released (0.004 MPa/min to 0 MPa) (3) and strain was recorded as ε_u(N), the temporary shape. Finally, the films were heated (2°C/min to T_m+~15°C) (4) to recover the permanent shape ε_p(N). This cycle was repeated at least three times to determine R_f and R_r. Notably, the 88%PCL-12%ACPCL film was deformed and recovered at 37°C, which was only ~3.5°C above its melting temperature (versus 15°C above T_m for other films).

Table 5: Shape Memory Properties of various films

Composition	X_G [%][1]	M_c [Da]	T_m [°C]	ε_1(N) [%]	R_r(1) [%]	R_r(N) [%]	R_f(N) [%]
100%PCL-DMA	61.7 ± 1.8	23.3	46.4 ± 2.6	14.1	99.7 ± 0.1	99.5 ± 1.4	98.3 ± 1.5
96%PCL-04%ACPCL	36.7 ± 8.6	37.9	45.4 ± 0.2	122.1	99.9 ± 0.2	99.8 ± 0.4	99.8 ± 0.1
	63.0 ± 8.6	37.3	43.4 ± 1.2	9.6	99.4 ± 0.8	99.4 ± 1.3	94.2 ± 1.2
94%PCL-06%ACPCL	60.3 ± 21.3	66.2	37.9 ± 0.9	8.3	93.7 ± 0.9	98.5 ± 0.6	98.7 ± 0.3
92%PCL-08%ACPCL	73.2 ± 12.0	74.9	39.0 ± 0.3	6.0	86.3 ± 3.3	98.0 ± 2.3	98.7 ± 1.8
89.4%PCL-	49.0 ± 6.2	62.9	37.9 ± 0.7	40.8	97.4 ± 0.7	99.7 ± 0.7	99.8 ± 0.2
10.6%ACPCL	78.2 ± 0.6	323.6	27.5 ± 3.0	6.2	90.8 ± 3.1	100 ± 5.3	92.5 ± 1.9
89%PCL-11%ACPCL	71.2 ± 6.7	155.4	35.1 ± 0.5	7.8	64.3 ± 7.0	92.5 ± 9.4	99.1 ± 0.6
88%PCL-12%ACPCL	64.1 ± 3.1	69.0	33.4 ± 1.2	14.6	99.9 ± 9.2	99.0 ± 6.2	98.8 ± 0.9
85%PCL-15%ACPCL	50.3 ± 2.5	300.5	29.7 ± 0.2	7.1	60.1 ± 0.6	86.9 ± 4.7	99.6 ± 0.2

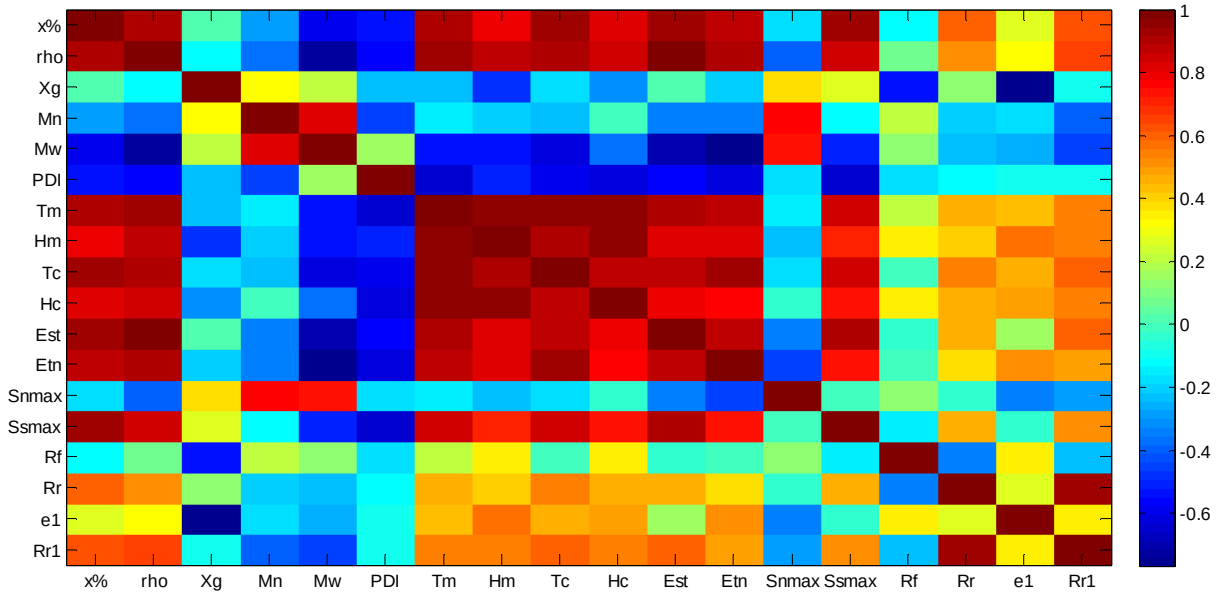

Figure 11: Heat map of PCA analysis demonstrating degree of covariance between chemical, physical, thermal, mechanical, and shape memory properties for SMP films. The degree of covariance between properties is indicated by the color map, indicating the nature (positive or negative) and degree (darkness) of correlation between the variables. Dark red indicates a strong positive correlation (up to 1.0) and dark blue indicates a strong negative correlation (up to 0.65). R_f(N) correlates most with x%PCL, R_r(1) correlates most with ρ, and R_f(N) and ε_1(N) depend most on X_G.

Shape memory behavior was demonstrated macroscopically by heating above T_m in a water bath, applying strain with tweezers, cooling in an ice bath, and heating above T_m in a water bath. Figure 12 shows three such original, temporary, and permanent shapes from three such deformations. Parts (B) to (C) show recovery of a tubular shape from an elongated thread-like shape at 37°C, indicating that the desired transformation for this vascular bypass graft surgery is attainable with these materials. Moreover, the elongated thread-like shape can be placed inside a catheter or laparoscope for minimally-invasive deployment in a wide variety of applications. Other transformations such as corkscrew to tube (D - F) and crumpled, cortorted piece to guitar (G – I) illustrate the excellent shape memory capabilities of these materials.

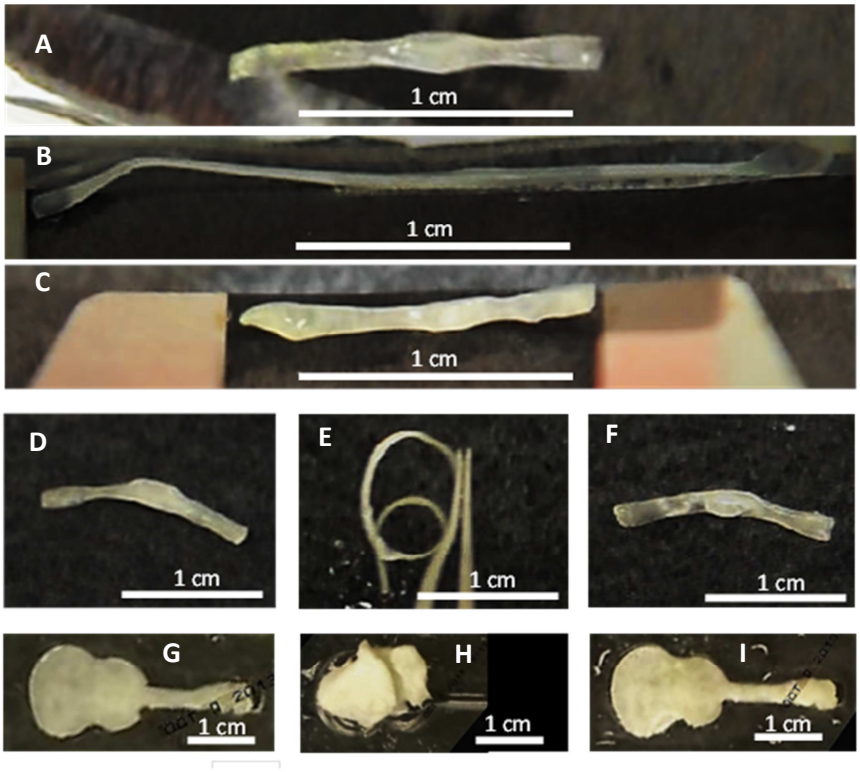

Figure 12: Shape Memory Demonstrations. 88%PCL-12%ACPCL tubular permanent shape (A) is deformed into a thread by heating at 50°C and applying strain (B). Heating at 37°C results in recovery of original, permanent tube shape (C). 88%PCL-12%ACPCL Tube (A) is deformed into corkscrew wire shape at 50°C, fixed at 4°C (E), and heated to 37°C to recover the original tubular shape (F). 92%PCL-08%ACPCL guitar (G) is heated to 50°C, strained, cortorted, and fixed at 4°C (H) before ultimate recovery of the guitar shape at 48°C.

In vitro degradation

In vitro degradation profiles were also assessed for the SMP films. As Appendix M shows, there were no statistically significant differences in degradation observed between the films over the course of 127 days. Mass remaining over this time course falls between 83 and 100%, indicating that there was no significant mass loss for this SMP library after 127 days. Similar to PCL, significant mass loss is not expected in the first year.

In vitro biocompatibility of SMP Films

Cell viability of HUVECs was first tested to determine if there were any toxic components leaching from films. To assess this, cells were seeded on TCPS and co-incubated with copolymer films and 100%PCL as a control. As Appendix M indicates, HUVEC viability was either statistically similar or better on polymer films than on the TCPS control and all were better than direct seeding on 100%PCL films at 35 and 91 hours post-incubation. Moreover, the cell viability values of HUVECs co-incubated with copolymer films, with the exception of 92%PCL-08%ACPCL, were statistically similar to those of HUVECs co-incubated with 100%PCL films. It is unclear why 92%PCL-08%ACPCL films would result in less cell viability, but the cell viability of HUVECs co-incubated with these films were not significantly different from that of HUVECs on TCPS, toimplying that there are not any legitimate concerns with this particular

copolymer composition. Together, these viability results indicate that there are no toxic leachables being released by the copolymer films after successive ethanol washes.

Direct seeding of cells on copolymer and 100%PCL films was used to investigate how cells proliferate on these materials. PCL has been widely proven to biocompatible [108, 109]. As Figure 13 indicates, HUVEC viability values on all test copolymer films were equivalent to or better than those on 100%PCL films. Lower cell attachment was observed on 92%PCL-08%ACPCL, which may be a function of a distinct material property (e.g. surface roughness), small tears in the film, or simply a result of the inherent limitations of the seeding procedure utilized. The seeding procedure could not ensure equivalent attachment to all polymer films and TCPS plates, as some cells undoubtedly did not attach to the film surfaces in the 1.5 hours allowed and were displaced and physically excluded from attachment when more media was added to the films in the wells. Cells that were displaced from the films after more media was added would have far lower viability as the surrounding 1% agarose coating prevents protein adsorption and cell attachment. This inherent procedural flaw may be why HUVEC viability is lower on all of the polymer films at 9 hours than it is for TCPS. Despite these complications, this experiment demonstrated that HUVEC viability on these copolymer films is equivalent to or better than the biocompatible PCL.

Confocal microscopy was utilized to assess morphology of hCAECs seeded on films after 3 days. As shown in Figure 14, ECs on all films and TCPS exhibit the trademark cobblestone morphology after 3 days, corroborating the positive viability results attained by the resazurin assay.

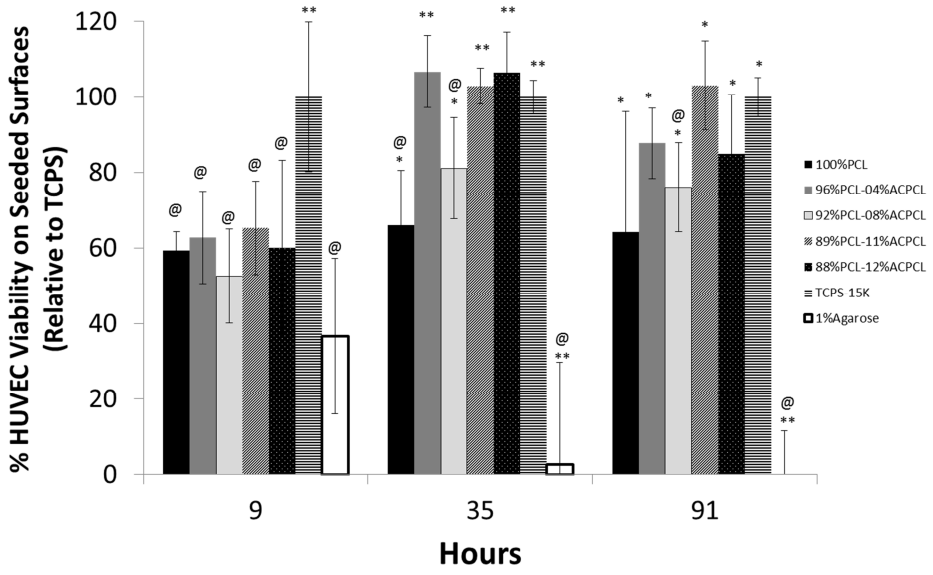

Figure 13: HUVEC viability on copolymer surfaces. Viability of HUVECs seeded directly on polymer surfaces at specified timepoints, where @ = significantly different from TCPS, * = significantly different from 1% agarose, and ** = significantly different from 100%PCL and 1% agarose (unless located above the 1% agarose bar). At 9 hours, HUVEC viability is lower on films than TCPS, which may be a result of insufficient cell attachment. At 35 hours, HUVECs on all but one copolymer film were significantly more viable than on 100%PCL. There was no significant difference to the TCPS control for all but one copolymer at 35 and 91 hours.

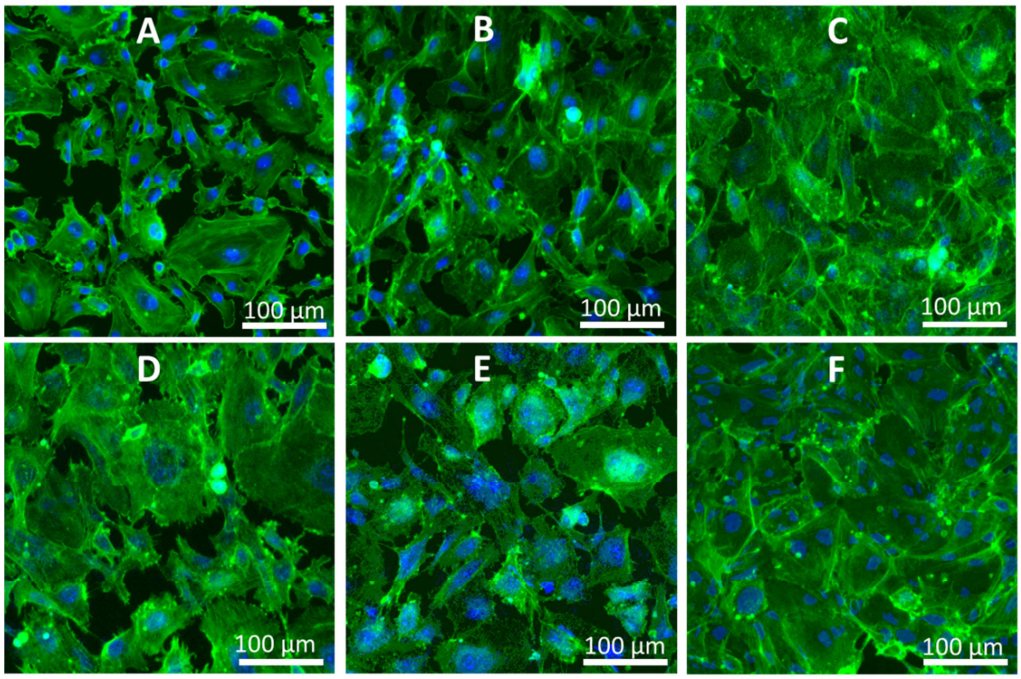

Figure 14: Human coronary artery endothelial cells (hCAECs) Morphology after 3 days. Confocal microscopy images of hCAECs seeded on TCPS (A), 100%PCL (B), 96%PCL-04%ACPCL (C), 92%PCL-08%ACPCL (D), 89%PCL-11%ACPCL (E), and 88%PCL-12%ACPCL (F) after 3 days exhibit trademark cobblestone morphology (Green: F-actin, Blue: Nuclei).

***In vivo* vascular bypass graft experiment**

A preliminary, proof-of-concept experiment was conducted *in vivo* to determine whether a PCL-ACPCL copolymer tube was capable of integrating into the native vasculature by providing a conduit for blood flow past an occluded region. The right common carotid artery of rats was ligated at two locations to induce severe occlusion, and in three of the rats ("Polymer + Peptide" group) the 89.4%PCL-10.6%ACPCL tube with two closed ends was immediately implanted and sutured in its permanent shape past each ligature such that the entire occluded area was covered by the polymer construct. The occluded region containing the polymer tube was treated with a pre-prepared collagen gel containing pro-angiogenic C16 and anti-inflammatory Ac-SDKP peptides. In the "Peptide Only" group, only the collagen gel with pro-angiogenic, anti-inflammatory peptides was applied to the occluded region. After 2 weeks, fluorescent microangiography indicated more abundant capillary growth in the "Polymer + Peptide" group (Figure 16A-B) than the "Peptide Only" group (Figure 16C-D), with vessels only visible around the ligation in the untreated group (Figure 16E) indicating near-complete occlusion without treatment [91]. Moreover, the very strong fluorescent signal from detection of fluorescent beads in Figure 16A-B indicated that blood perfused through the tubular construct. H&E staining (Figure 15C, Supplementary Figure 16A – C) illustrated that anastomosis and capillary connection occurred between polymer tube and native artery. These observations indicate that the tubular construct integrated into the native vascular via capillary connection with the occluded artery.

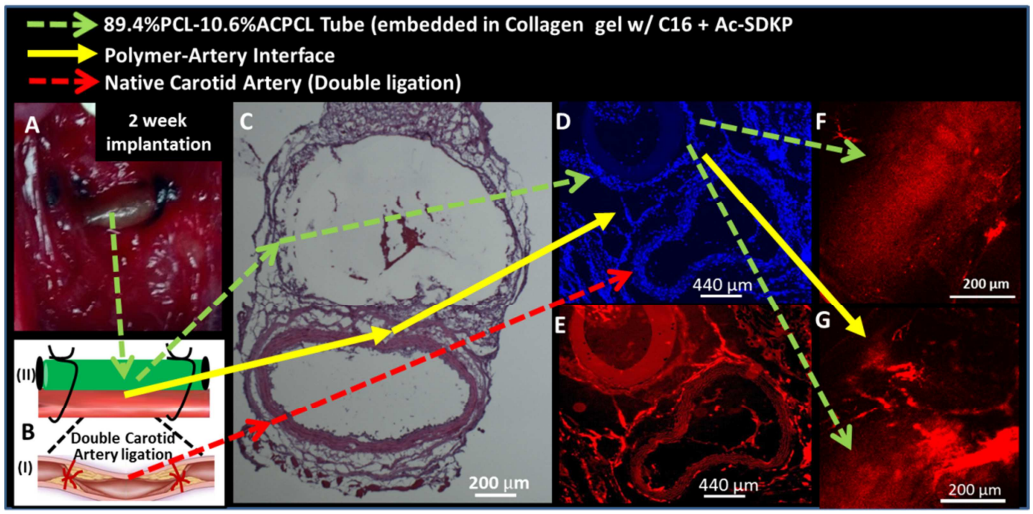

Figure 15: Overview of bypass graft results for "Polymer + Peptide" treated group. (A) Picture of SMP during implantation. **(B)** Diagram of surgical procedure in which (I) two ligatures were applied to the right carotid artery and (II) a 89.4%PCL-10.6%ACPCL SMP tube implanted at site of occlusion was sutured and embedded with a collagen gel containing peptides. **(C)** H&E staining illustrates relation between polymer (top) and native artery (bottom). **(D)** Hoechst (blue) and **(E)** CD31 (red) staining of polymer-artery interface. **(F-G)** Confocal images from fluorescence microangiography of the polymer tube.

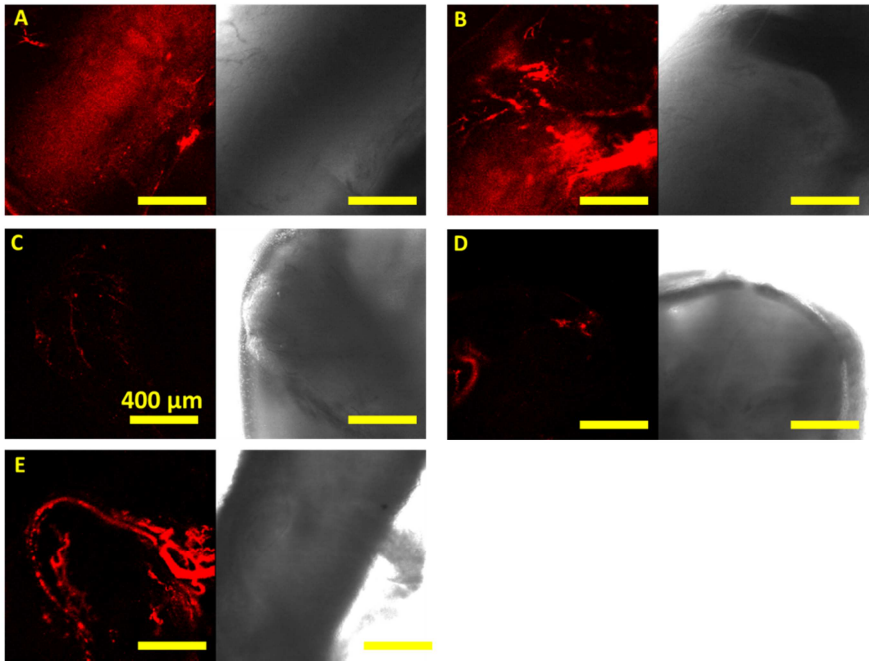

Figure 16: Fluorescence Microangiography Images from Grafting Experiment. (A,B) "Polymer + Peptide"; (C,D) "Peptide Only"; (E) untreated ligatures.

Discussion

A novel SMP library was generated with the intent of treating occluded arteries using a surgically favorable grafting procedure. SMPs are advantageous for this application because they can be implanted in a minimally-invasive manner, while also possessing favorable biocompatible and bioresorbability features. First, the novel x%PCL-y%ACPCL copolymer library was synthesized via ROP of CL with novel monomer ACCL. Molar composition varied from y = 4.16 – 17.86% and was controlled by the monomer feed ratio (CL:ACCL), while molecular weight characteristics were dependent upon the initiator:monomer ratio as well as the distribution of diethylzinc catalyst. Number-average molecular weight (M_n) ranged from 12.1 – 29.7 kDa for y = 4.16 – 14.5%, with PDI from 1.54 – 2.50. To better understand the dependence of thermal properties on molar composition and molecular weight characteristics, principal component analysis (PCA) was performed. From this analysis, it was concluded that prior to crosslinking, thermal properties depend most on molar composition and M_w.

SMP films were generated from these copolymers by photocrosslinking the pendant allyl groups between polymer chains. Melting temperatures (T_m's) were measured in order to determine the switch temperature, T_{sw}, required for shape recovery, and ranged from 45.4 – 28.6^{o}C for the subset of films studied. This range of melting temperatures is ideal for physiological applications. When it is desired to simply deploy the polymer to a site of interest to recover its shape, such as in deployment of a polymeric stent in occluded arteries, SMPs with $T_m \leq 37^oC$ are best as their permanent shape can be fully recovered upon implantation without additional heating [23]. In other lengthier, more invasive surgical procedures, it may be desired to delay the recovery of the permanent shape until implantation is complete [29]. In this scenario, SMPs with T_m just above 37^{o}C are a more appropriate choice as shape recovery can be actuated when desired by a mild heating procedure. Development of this novel SMP library provides the capability to tune material parameters to best match a particular application or situation.

Based on a plot of thermal properties versus y%ACPCL, it is obvious that there is a strong correlation between molar composition and thermal properties. However, other variables, such as molecular weight characteristics, varied for each copolymer. To more precisely define the relationship between thermal properties and chemical and physical parameters, PCA was performed on the data subset. This analysis revealed that the crosslinking density, ρ, correlated strongest with T_m, even more so than x%PCL, which is consistent with trend in other highly crosslinked networks [105].

Mechanical, contact angle, and shape memory properties were assessed for the copolymer films. Analysis of mechanical properties suggests that these materials are of seemingly appropriate elasticity and ductility for vascular applications to avoid issues that arise from compliance mismatches such as thrombogenicity and impaired reendothelialization [24, 106, 110]. Tensile moduli at 37^{o}C, E_{tn}'(37^{o}C), varied between 75.9 – 2.2 MPa for the copolymer films, with strain to break, ε_{max}, greater than 100% for most films. Like PCL, these copolymer films are hydrophobic, with contact angles ranging from 70^o – 83.5^o. Shape memory properties of the copolymer films were excellent, with shape fixity and shape recovery >98% for most compositions. Adjusting X_G apears to improve shape fixity, while reduction in the fixing temperature can likely improve shape recovery for higher y%ACPCL copolymers.

This copolymerization and crosslinking methodology enables tuning of these melting temperatures as well as important mechanical properties. It was desired to elucidate the correlations between these variables in order to tailor materials to specific vascular applications.

The 89.4%PCL-10.6%ACPCL SMP tube was implanted in a double carotid artery ligation and embedded in a collagen gel containing pro-angiogenic C16 and anti-inflammatory Ac-SDKP peptides in

order to assess the feasibility of this approach for treating CAD and other vascular diseases. After just 2 weeks, capillary formation occurred between the SMP tube and the native artery and appeared to have promising effects in rescuing a severely occluded carotid artery. Notably, angiogenesis is far more prominent in the “Polymer + Peptide” group and fluorescence microangiography images demonstrate that the tube was integrated in the perfused vascular system within this 2 week timeframe. Of course, further studies are required to verify and quantify these phenomena to optimize this therapeutic approach. Key points to address include quantification of blood flow through the tubular constructs, improved endothelialization, and repair of already occluded areas. Nonetheless, this surgically advantageous bypass grafting procedure appears to be a promising technique for treatment in CAD.

Conclusions

A series of novel, physiologically-responsive x%PCL-y%ACPCL SMPs were produced with excellent shape memory properties and melting temperatures ranging from 45.4 – 28.6 ^{o}C. These films are elastic and ductile like PCL, but tended to have lower moduli in this study. PCA shows that thermal, mechanical, and shape memory properties can be further optimized for given y%ACPCL copolymers by increasing M_n and reducing M_w, PDI and X_G to achieve an even more versatile range of polymer characteristics. A 89.4%PCL-10.6%ACPCL SMP tube functionalized via embedding in a collagen gel with pro-angiogenic, anti-inflammatory peptides was able to form capillary connections to the native artery and provide a conduit (i.e. collateral blood vessel) for blood flow past a severely occluded region of the carotid artery after just 2 weeks. This study demonstrates the promise of this technique for treating CAD and the potential utility of these novel materials for other vascular applications.

APPENDIX

Appendix A: Synthetic Scheme of 100%PCL-dimethacrylate

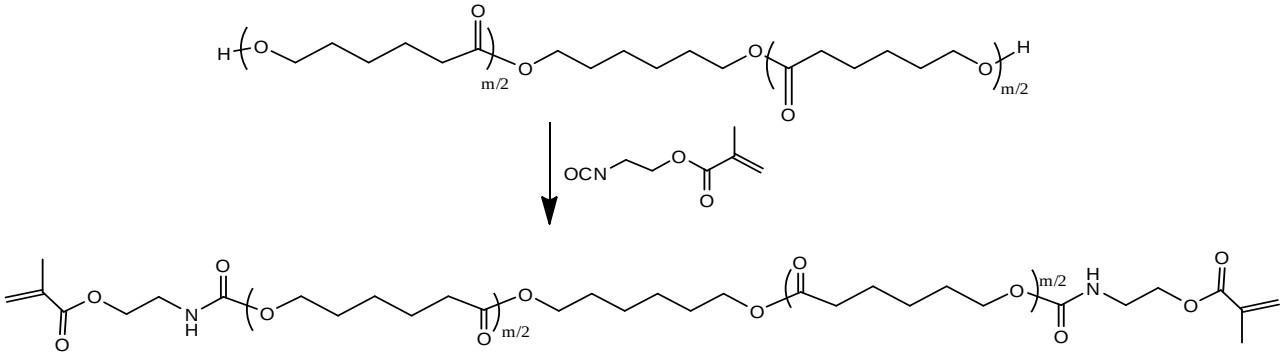

Supplementary Figure 1: Synthetic Scheme of 100%PCL-dimethacrylate. This polymer was synthesized as a control for comparison to x%PCL-y%ACPCL SMPs.

Appendix B: ^{1}H-NMR spectra of α-allyl carboxylate-ε-caprolactone (ACCL)

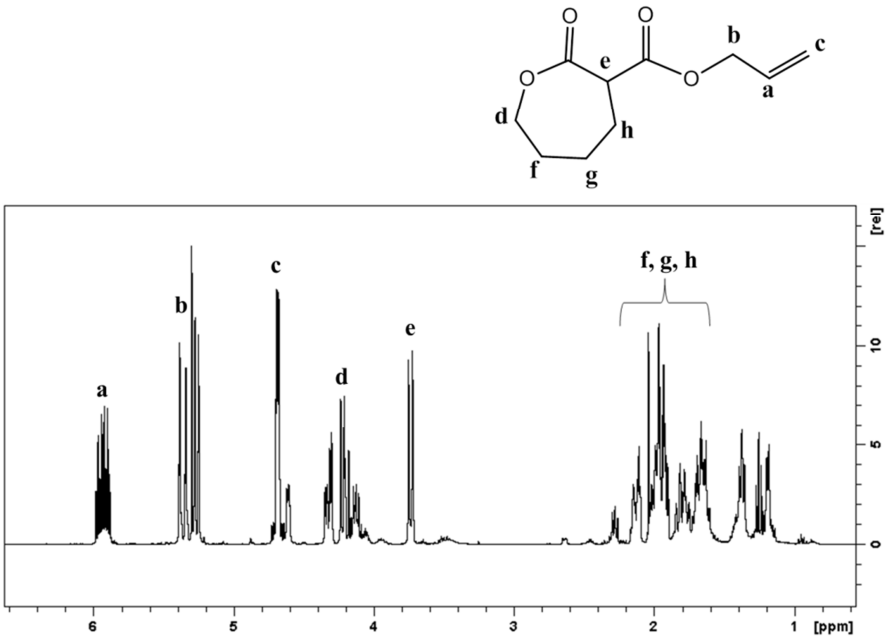

Supplementary Figure 2: ^{1}H-NMR spectra of ACCL. Peaks unique to ACCL are designated by letters a, b, c, and e.

Appendix C: Correlation between monomer feed ratio and molar composition of x%PCL-y%ACPCL copolymers

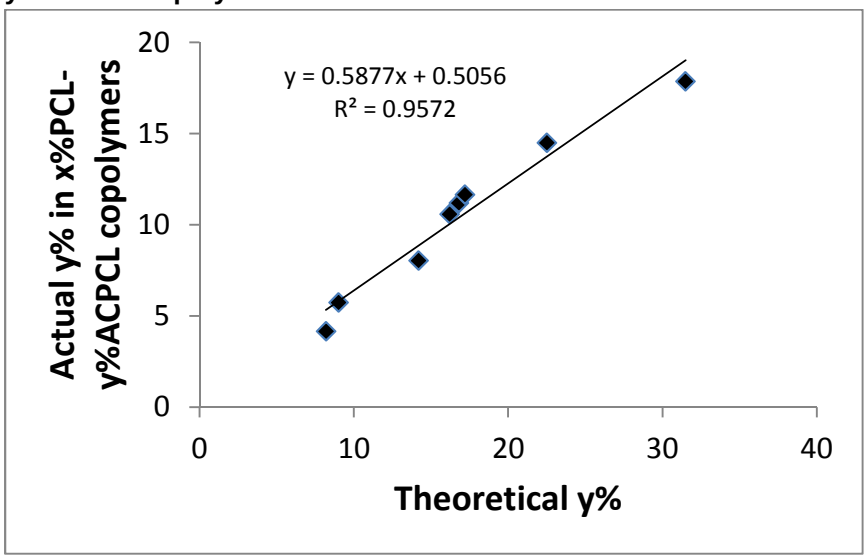

Supplementary Figure 3: Correlation between ACCL:CL monomer feed ratios and y%ACPCL achieved in x%PCL-y%ACPCL copolymers. There exists a good linear correlation between monomer feed ratio and molar composition of copolymers, indicating that monomer feed ratio can be used to finely tune copolymer compositions.

Appendix D: ^{1}H-NMR of α-allyl carboxylate-ε-caprolactone (ACCL)

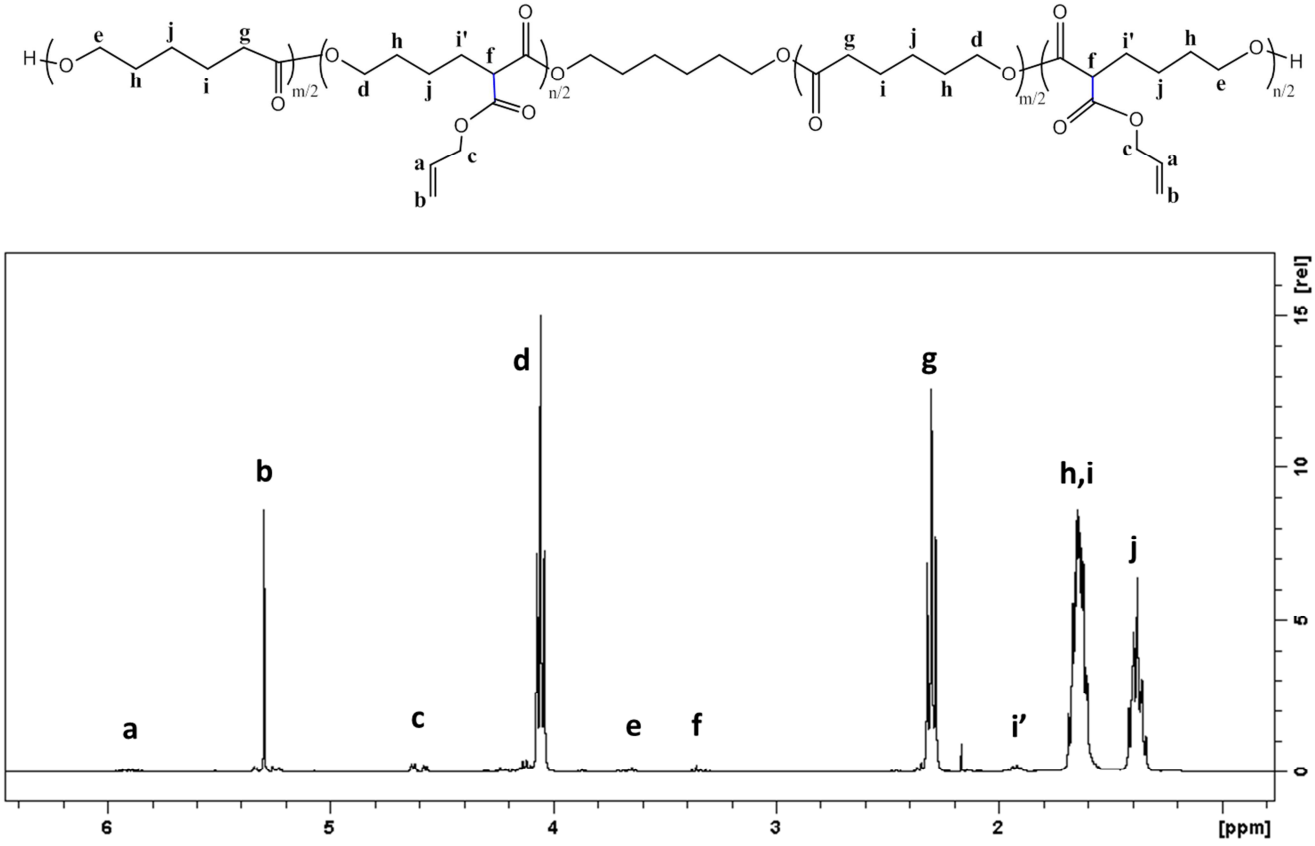

Supplementary Figure 4: ^{1}H-NMR spectra of 96%PCL-04%ACPCL. Peaks unique to allyl carboxylate (ACPCL) units are designated by letters a, b, f, and i'.

Appendix E: Table of Copolymer Color and Consistency

Supplementary Figure 5: Table of Copolymer Color and Consistency as a function of y% and molecular weight. Most copolymers were powders, but copolymers with the highest M_w were powders intermixed with transparent film fragments and low molecular weight y=17.86% was a slurry at room temperature. Molar composition and PDI determined how much red-orange was incorporated in the polymer.

Polymer	Color and consistency	Actual y [%]	M_n [Da]	M_w [Da]	PDI
96%PCL-04%ACPCL	White powder	4.16	15060	26870	1.78
94%PCL-06%ACPCL	Yellow-orange powder intermixed with clear film	5.74	16546	39050	2.36
92%PCL-08%ACPCL	White powder	8.04	22026	35074	1.59
89.4%PCL-10.6%ACPCL	Light orange powder	10.58	13627	34049	2.50
89%PCL-11%ACPCL	Yellow-white powder intermixed with clear film	11.20	29709	48842	1.64
88%PCL-12%ACPCL	Yellow powder	11.66	19087	36430	1.91
85%PCL-15%ACPCL	Red-orange powder	14.50	12095	28931	2.39
82%PCL-18%ACPCL	Red-orange slurry	17.86	8375	19987	2.39

Supplementary Figure 6: Appearance of x%PCL-y%ACPCL, from left to right, in order of increasing ACPCL content.

Appendix F: Molecular Weight of 100%PCL-dimethacrylate

Supplementary Figure 7: Molecular Weight information for 100%PCL-dimethacrylate control.

Polymer	**M_n [Da]**	**M_w [Da]**	**PDI**
100%PCL	11300	17368	1.54
100%PCL-DMA	11628	16417	1.41

Appendix G: Dependence of Thermal properties of Copolymers on Molar composition and molecular weight

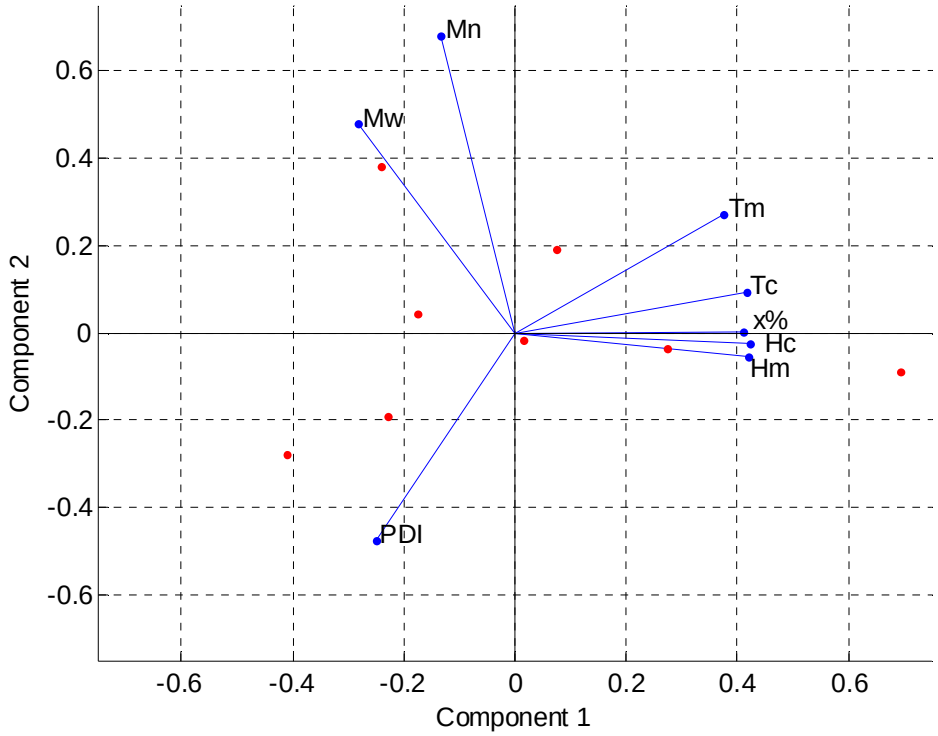

Supplementary Figure 8: 2D Plot of variable contributions to first 2 components. These two principal components account for 69.4% and 24.2% of the system covariance, respectively (93.6% cumulative). The first principal component is almost perfectly aligned with x%PCL, indicating a very significant contribution of this variable. Meanwhile the second component is completely independent of this first component and is mostly tied to molecular weight characteristics. Thermal properties appear to be mostly tied to x%PCL, although molecular weight characteristics are also an influence as judged by the non-zero y-position of these vectors.

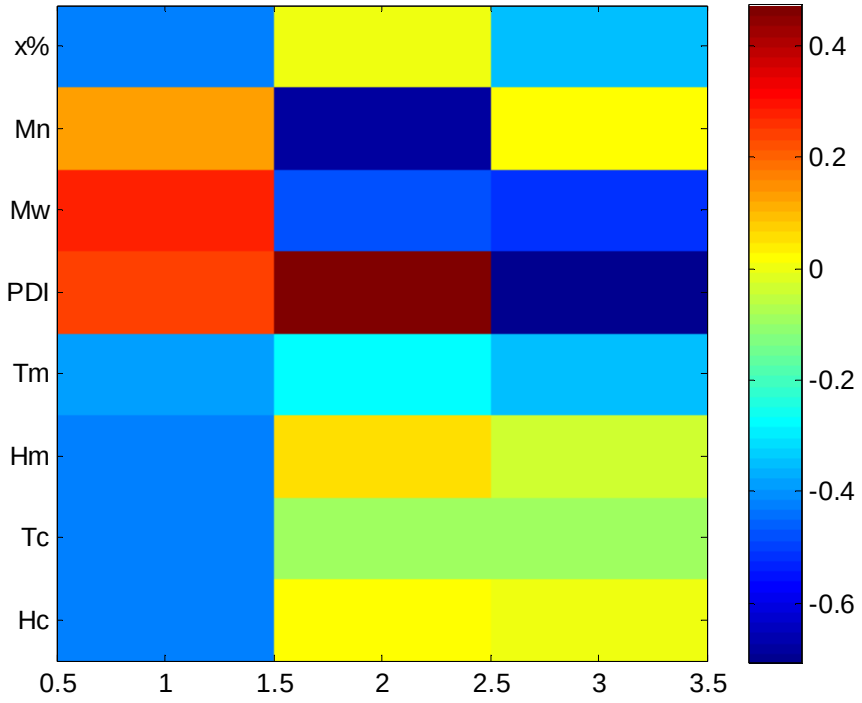

Supplementary Figure 9: Contribution of variables to principal components. The contribution of variables to principal components 1, 2, and 3 is displayed columns 1, 2, and 3, respectively. These components account for 69.4, 24.2, and 5.4% (99.0% cumulative) of the variance, respectively. Thus, variables contributing most to the first component account for the greatest proportion of variance in the system. Darker colors indicate a greater contribution to principal components. Based on this representation, independent variables x%PCL and M_w contribute most to the variance, while dependent variables ΔH_m, T_c, and ΔH_c also account for the majority of the system's covariance (T_m to a lesser extent).

Appendix H: Dependence of Thermal Properties of SMPs on Chemical and Physical Properties of SMP Films

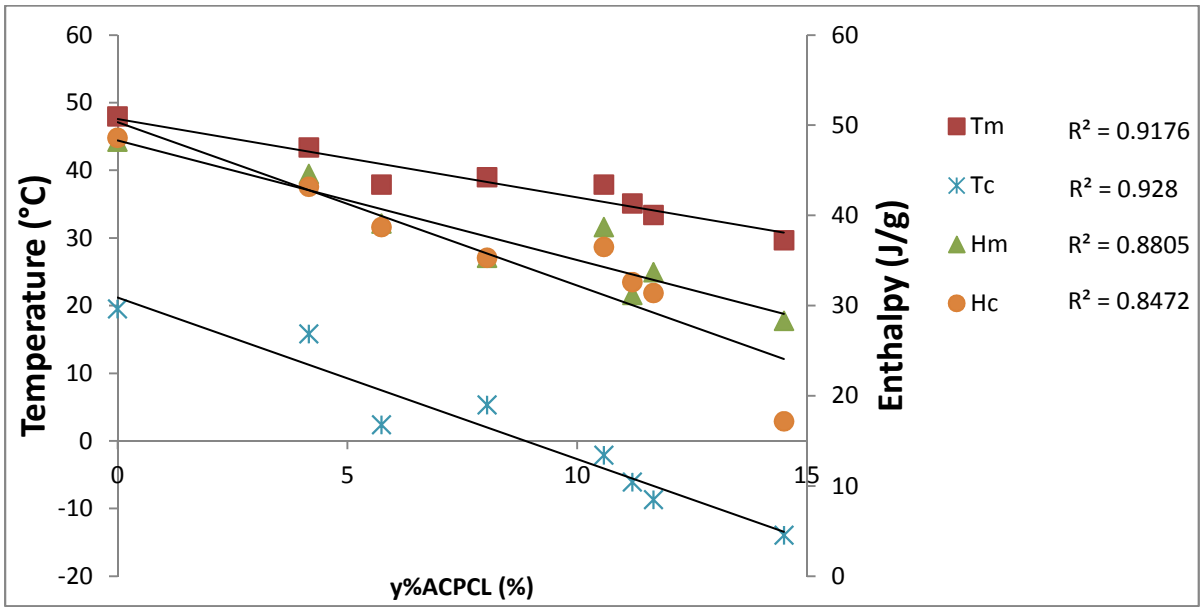

Supplementary Figure 10: Dependence of thermal properties on molar composition for SMP films.

63.58, 83.87, 95.20, 98.58

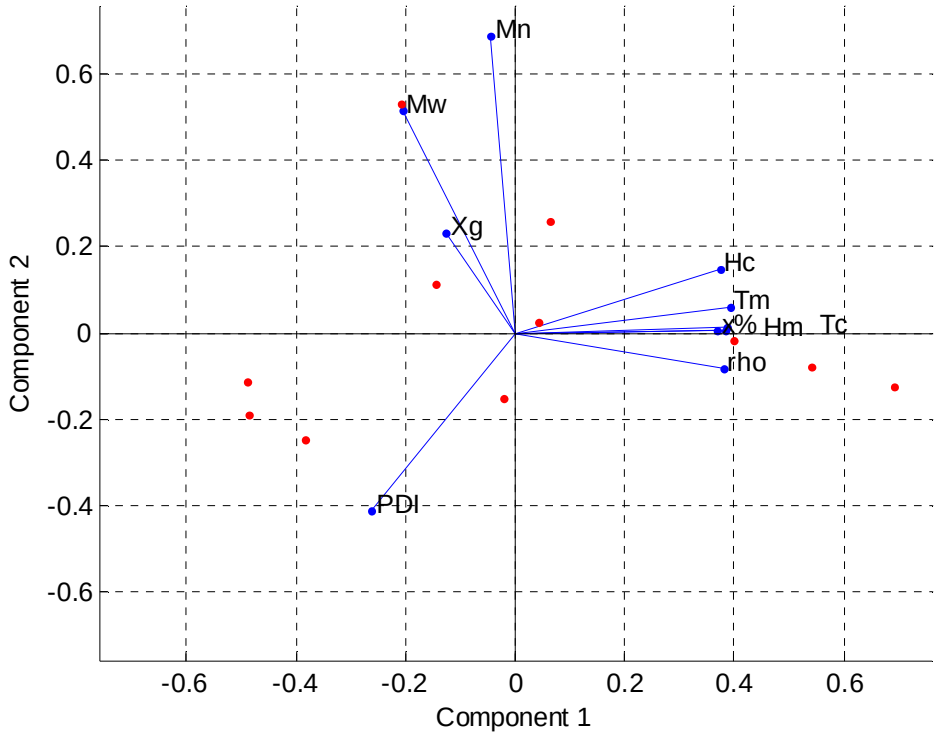
Mn
Mw
Xg
Hc
Tm
x%
Hm
Tc
rho
PDI
0.6
0.4
0.2
0
-0.2
-0.4
-0.6
Component 2
Component 1

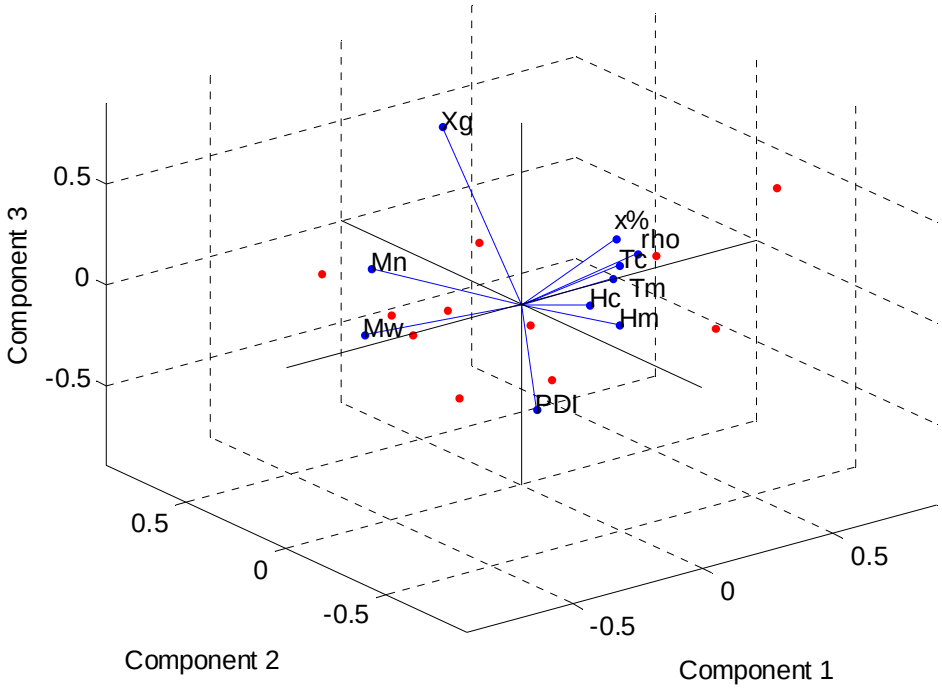
Xg
x%
rho
Tc
Mn
Tm
Hc
Hm
Mw
PDI
0.5
0
-0.5
Component 3
Component 2
Component 1

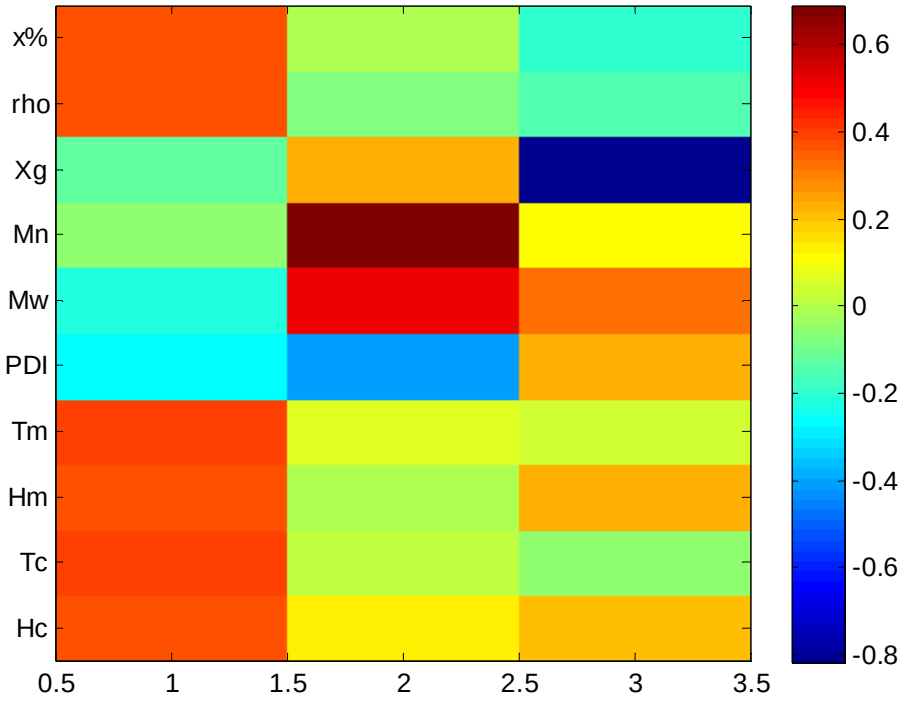
x%
rho
Xg
Mn
Mw
PDI
Tm
Hm
Tc
Hc
0.5
1
1.5
2
2.5
3
3.5
0.6
0.4
0.2
0
-0.2
-0.4
-0.6
-0.8

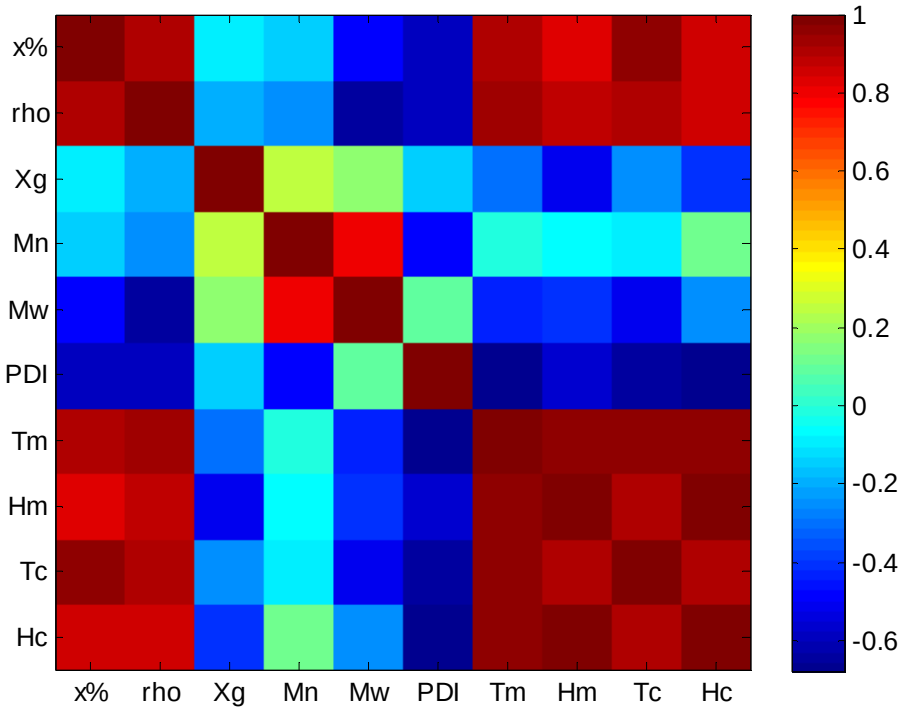
x%
rho
Xg
Mn
Mw
PDI
Tm
Hm
Tc
Hc
x%
rho
Xg
Mn
Mw
PDI
Tm
Hm
Tc
Hc
1
0.8
0.6
0.4
0.2
0
-0.2
-0.4
-0.6

Appendix I: Dependence of Mechanical Properties on Chemical and Physical Properties of SMP Films

63.71, 83.75, 93.23, 97.08

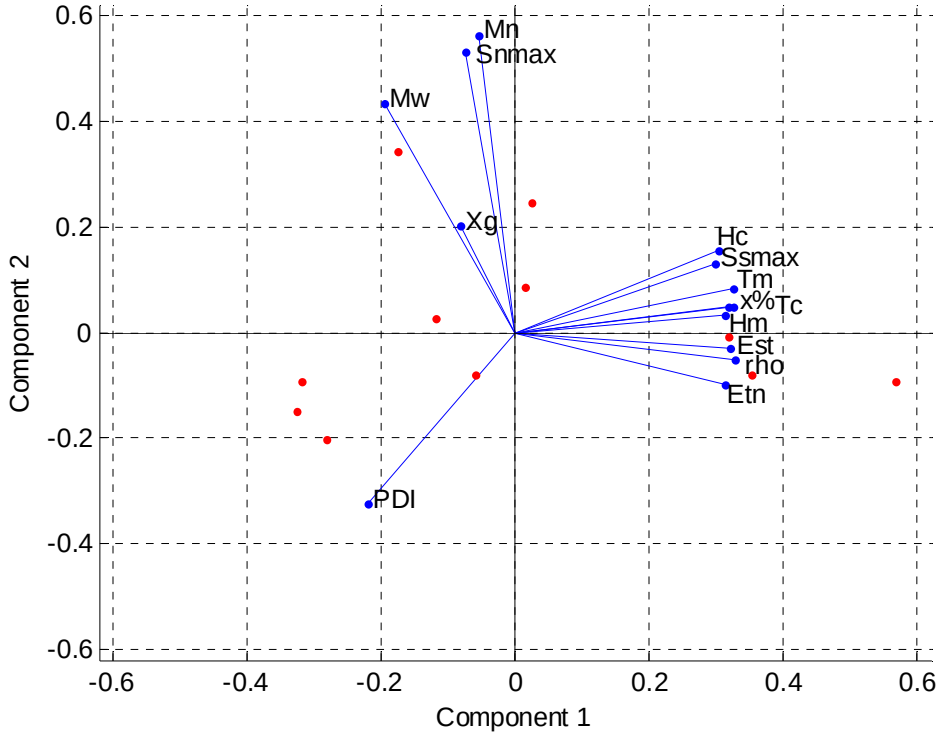

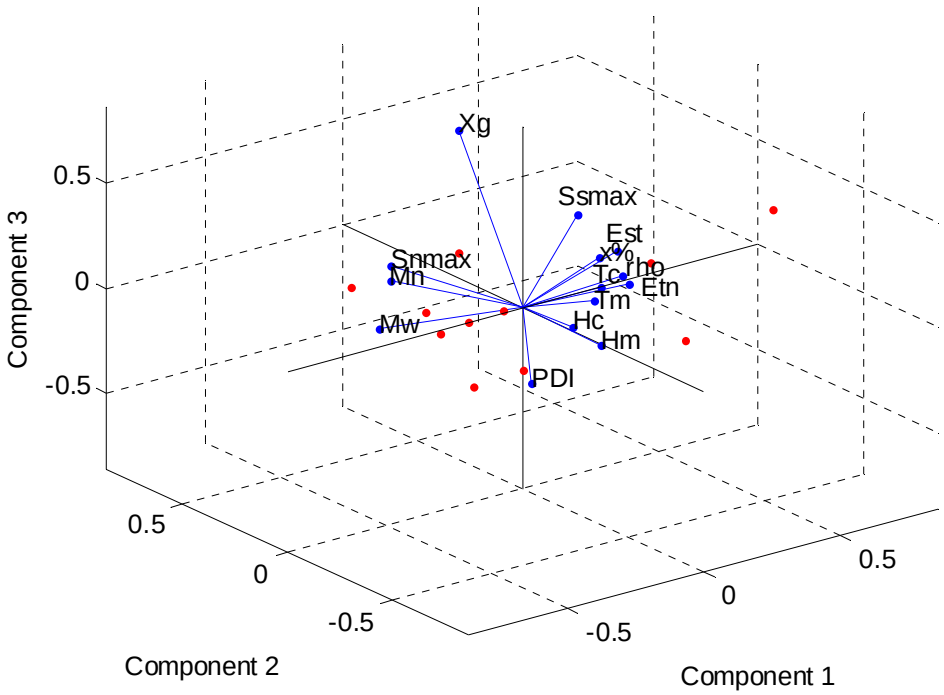
Xg
Ssmax
Est
x%
rho
Tc
Etn
Tm
Hc
Hm
Snmax
Mn
Mw
PDI
0.5
0
-0.5
Component 3
Component 2
Component 1

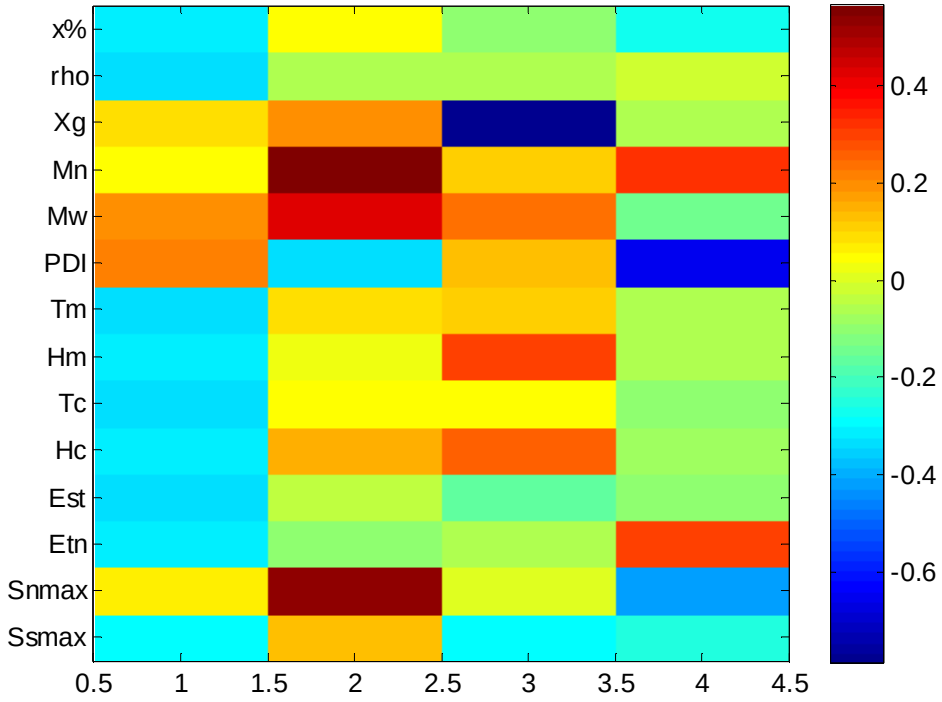
x%
rho
Xg
Mn
Mw
PDI
Tm
Hm
Tc
Hc
Est
Etn
Snmax
Ssmax
0.5
1
1.5
2
2.5
3
3.5
4
4.5
0.4
0.2
0
-0.2
-0.4
-0.6

Appendix J: Contact angle properties of SMP films

Supplementary Figure 11: Advanced contact angle in comparison to other material properties for various SMP films.

Composition	M_n [Da]	M_w [Da]	PDI	X_G [%]	M_c [Da]	T_m [^oC]	θ_{ADV} (^{o})
100%PCL-DMA	11628	16417	1.41	61.7 ± 1.8	23.3	46.4 ± 2.6	78.0 ± 14.5
96%PCL-04%ACPCL	15060	26870	1.78	36.7 ± 8.6 63.0 ± 8.6	37.9 37.3	45.4 ± 0.2 43.4 ± 1.2	73.8 ± 12.6 70.3 ± 4.6
94%PCL-06%ACPCL	16546	39050	2.36	60.3 ± 21.3	66.2	37.9 ± 0.9	80.0 ± 3.7
92%PCL-08%ACPCL	22026	35074	1.59	73.2 ± 12.0	74.9	39.0 ± 0.3	79.5 ± 5.1
89.4%PCL-10.6%ACPCL	13627	34049	2.50	49.0 ± 6.2 78.2 ± 0.6	62.9 323.6	37.9 ± 0.7 27.5 ± 3.0	81.5 ± 3.8 82.8 ± 6.8
89%PCL-11%ACPCL	29709	48842	1.64	71.2 ± 6.7	155.4	35.1 ± 0.5	70.5 ± 1.7
88%PCL-12%ACPCL	19087	36430	1.91	64.1 ± 3.1	69.0	33.4 ± 1.2	75.5 ± 2.9
85%PCL-15%ACPCL	12095	28931	2.39	50.3 ± 0.6	300.5	29.7 ± 0.2	83.5 ± 7.1

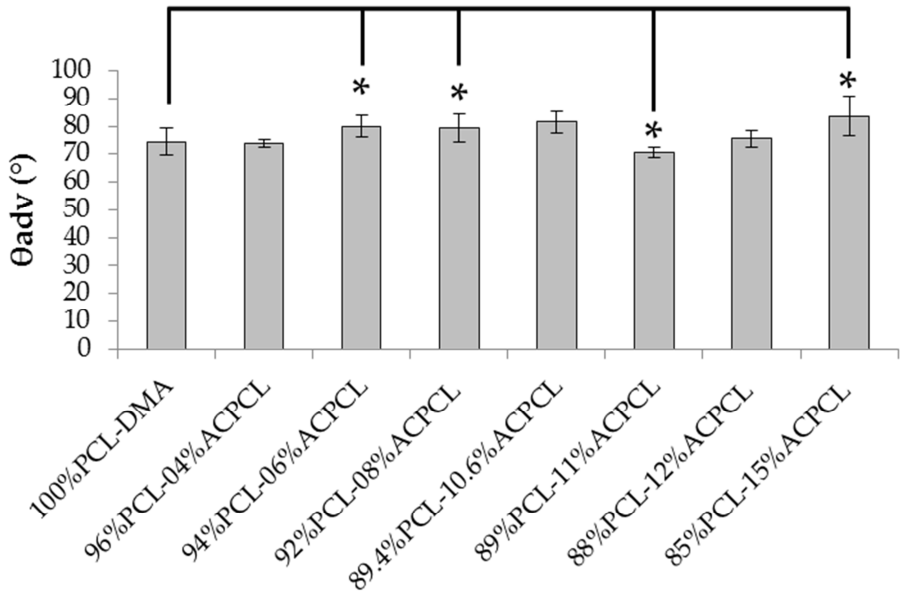

Supplementary Figure 12: Advanced Contact Angle of SMP films.

Appendix K: Dependence of Contact Angle on Chemical and Physical Properties of SMP Films
62.57, 81.68, 90.97, 96.22, 98.14

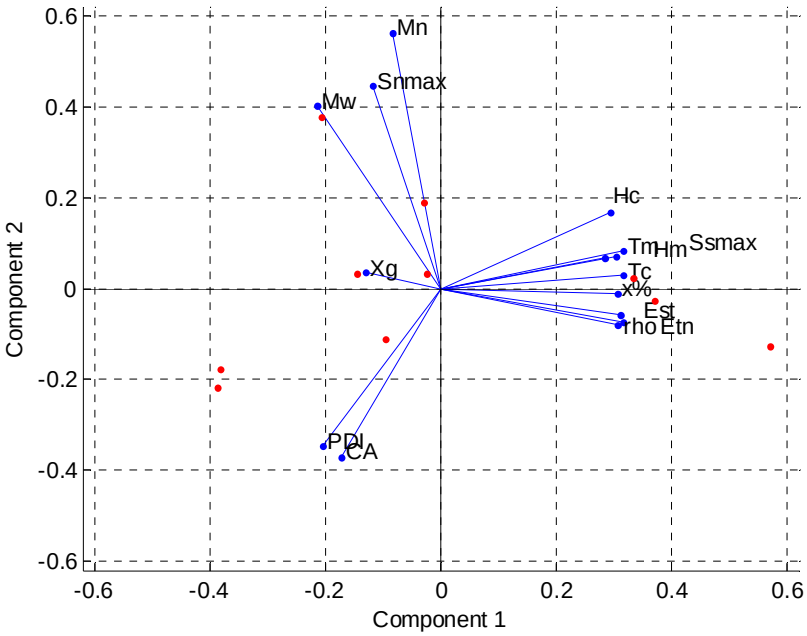

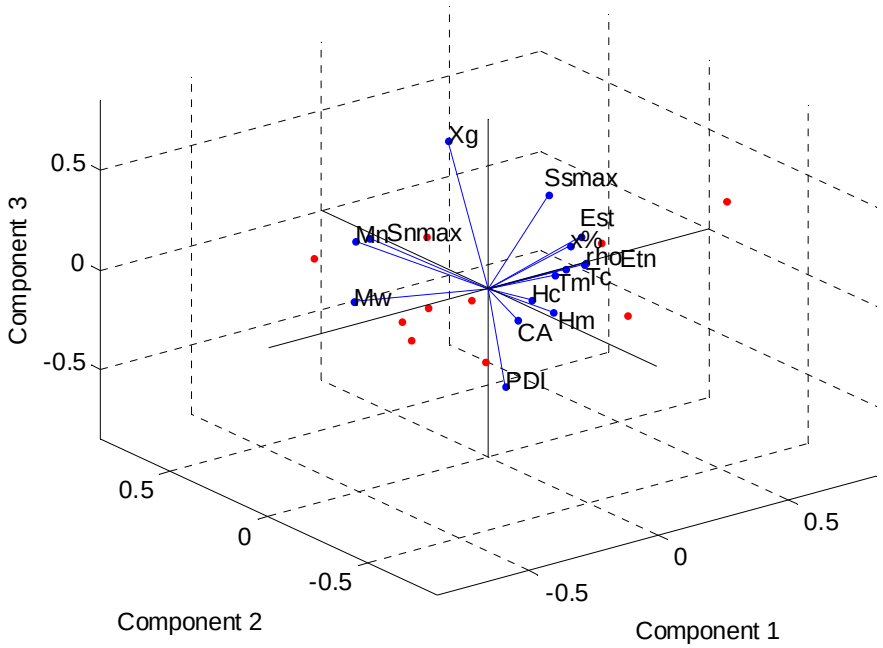
Component 3
0.5
0
-0.5
Xg
Ssmax
Est
x%
rho
Etn
Tm
Tc
Hc
Hm
CA
PDI
Mn
Snmax
Mw
0.5
0
-0.5
Component 2
0.5
0
-0.5
Component 1

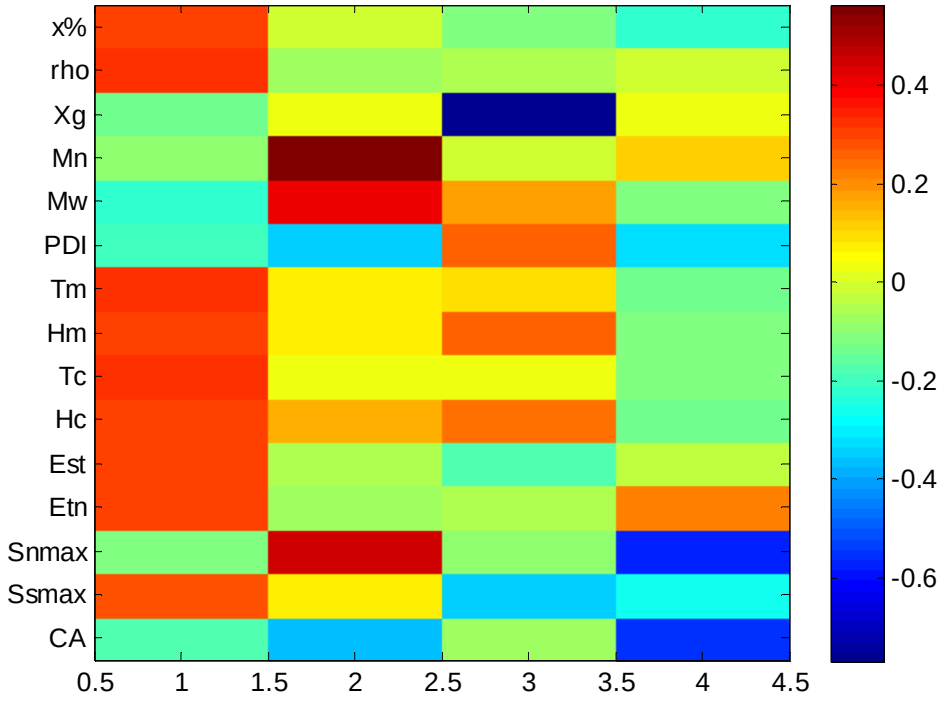
x%
rho
Xg
Mn
Mw
PDI
Tm
Hm
Tc
Hc
Est
Etn
Snmax
Ssmax
CA
0.5
1
1.5
2
2.5
3
3.5
4
4.5
0.4
0.2
0
-0.2
-0.4
-0.6

Appendix L: Correlation of Shape Memory Properties with Chemical and Physical Properties of SMP Films

54.73, 70.56, 84.27, 92.25, 95.84

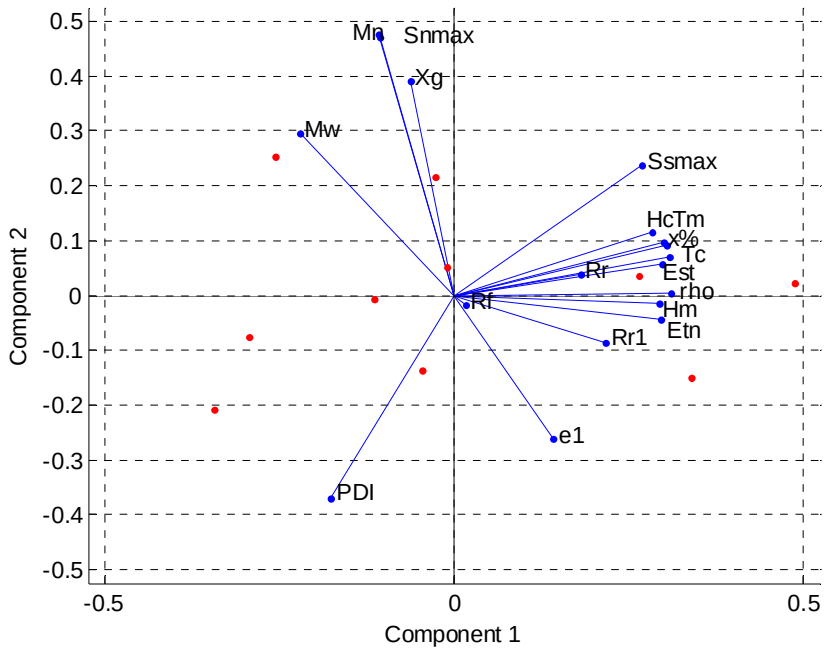

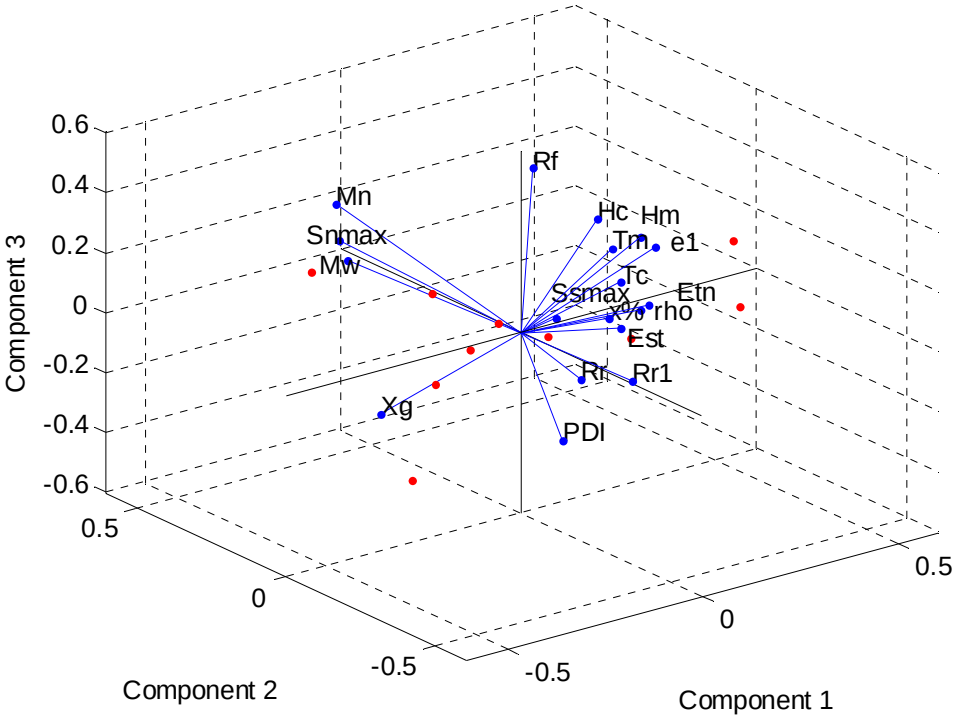

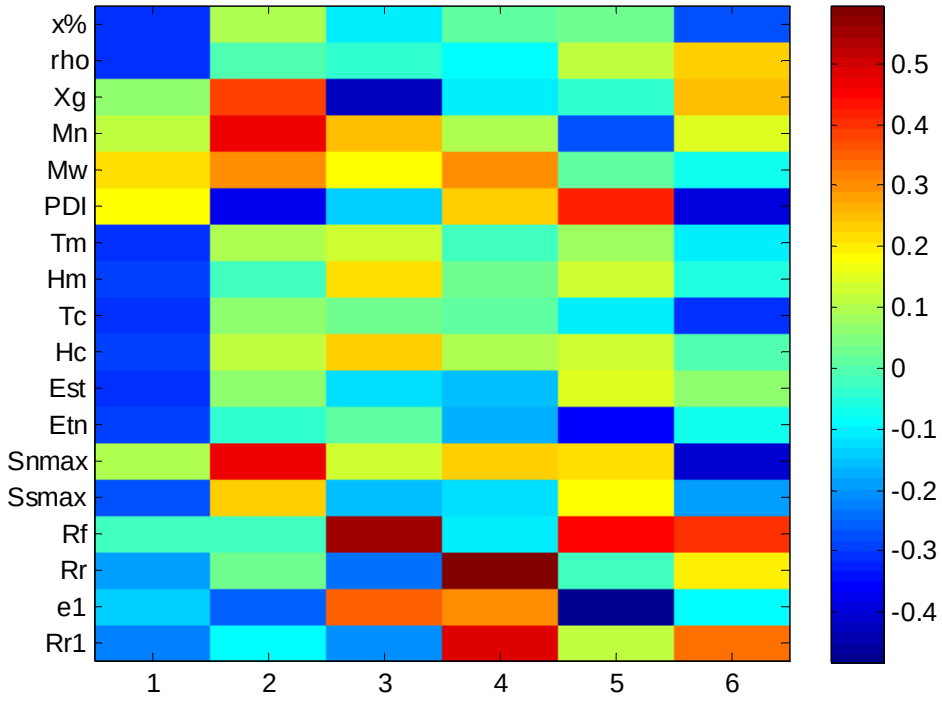

Appendix M: In vitro degradation of SMP films.

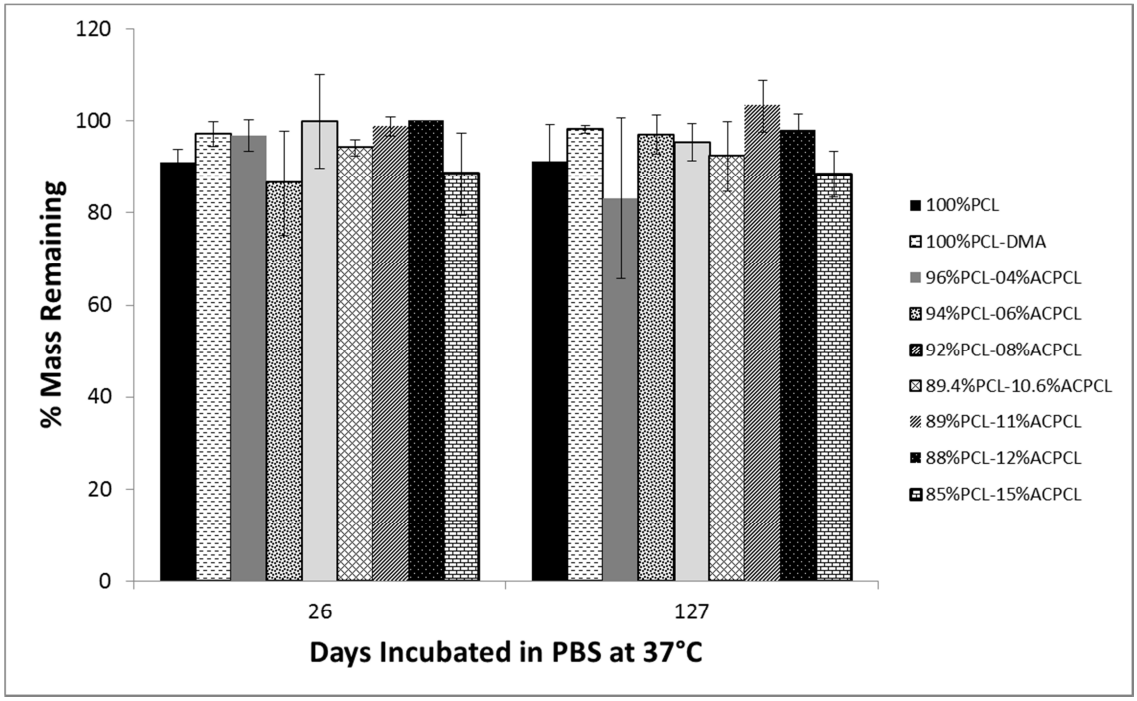

Supplementary Figure 13: In vitro degradation of SMP films.

Appendix N: Viability of HUVECs co-incubated with SMP films.

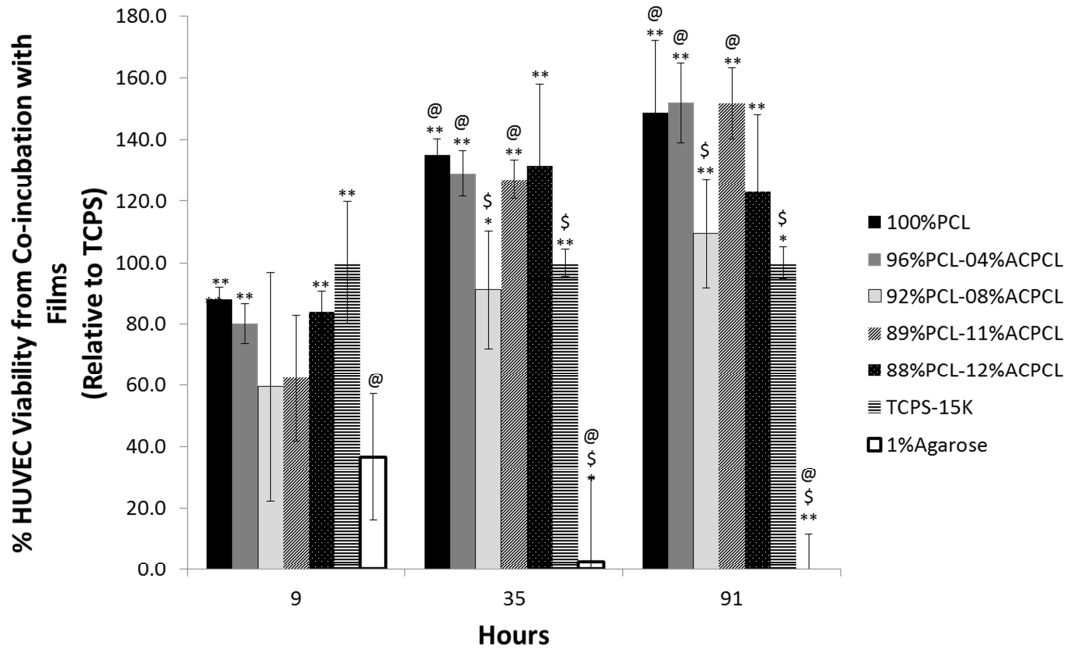

Supplementary Figure 14: HUVEC Viability co-incubated with films.

Appendix O: Supplementary images from *in vivo* Bypass Grafting Experiment

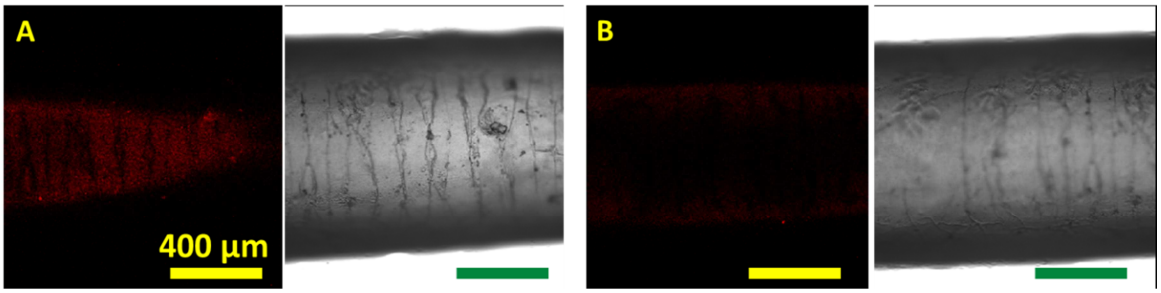

Supplementary Figure 15: SMP tube with no perfused beads. Autofluorescence from non-perfused 89.4%PCL-10.6%ACPCL is far less than perfused tubes (Figure 16A-B).

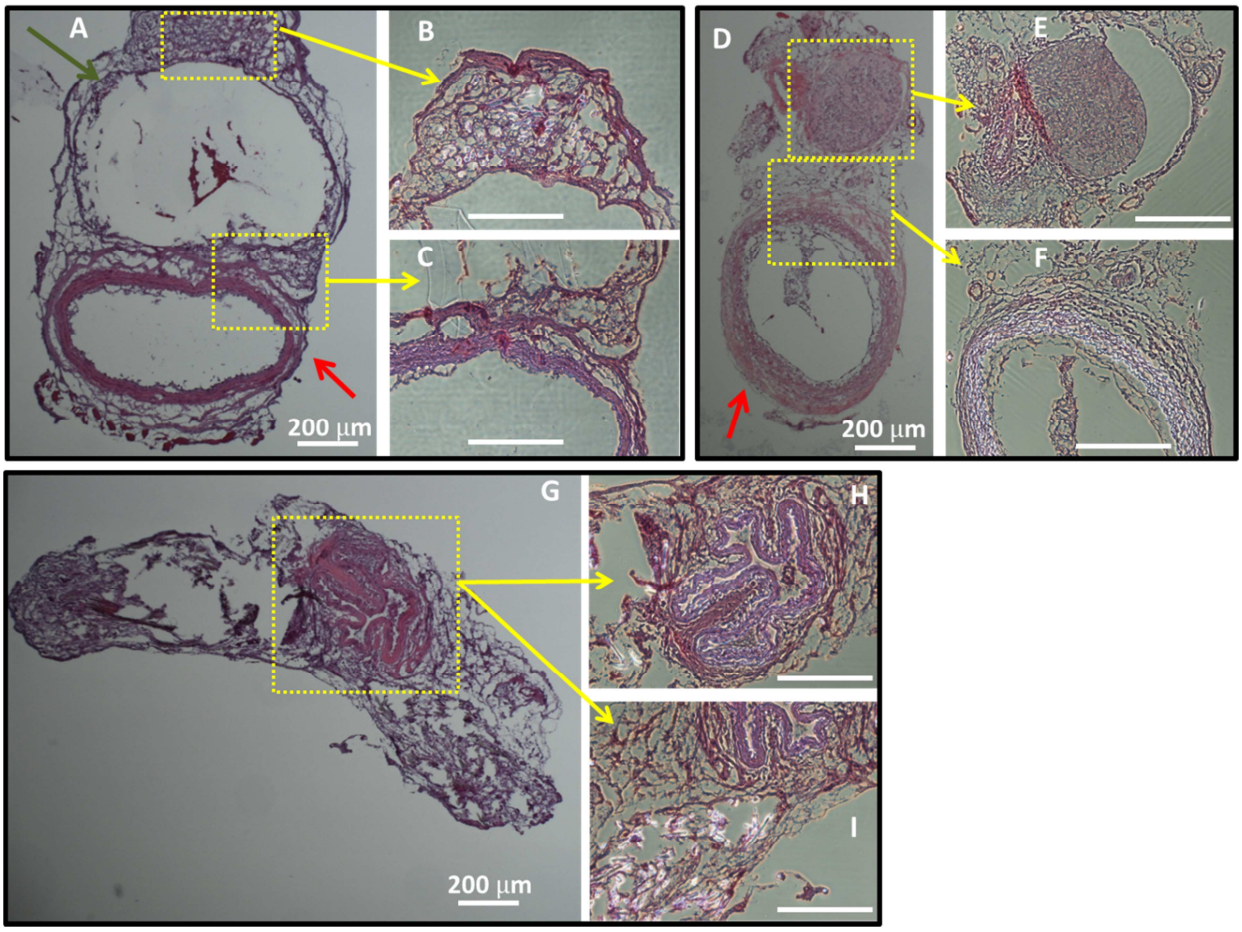

Supplementary Figure 16: H&E Staining of OCT sections. (A – C) In the polymer-treated artery, there appears to be a capillary connection between the polymer (top) and native artery (bottom) (A and C). Away from the interface with the artery, the polymer is less vascularized with more collagen deposits (B). (D – F) In the peptide only treated artery, there appear to be small collateral vessels formed (E and top of D), but this vascular network appears to be less organized than the polymer + peptide group in (A – C). (G – I) The untreated artery appears occluded (G, H), with possible atherosclerotic plaque formation (white spots) around the periphery of the occlusion (I).

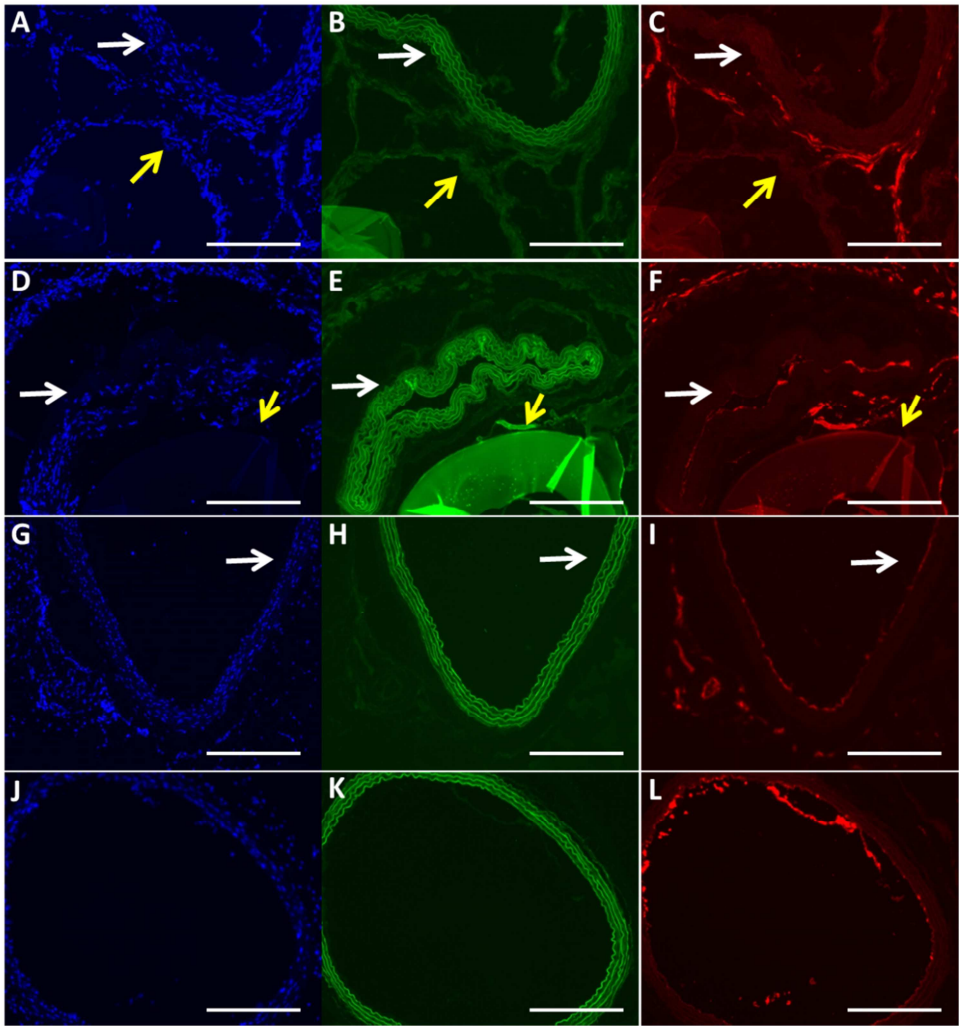

Supplementary Figure 17 : Immunofluorescent staining of polymer/artery OCT sections. White arrows and yellow arrows designate the native artery and polymer tube, respectively. Blue (left) indicates Hoechst nuclear stain, green (middle) is anti-CD45 leukocyte antigen, and red (right) is anti-CD31 endothelial cell marker. Images (A) – (I) were OCT sections from the polymer + peptide treated group, while (J) – (L) were images of OCT sections from the untreated group. (A) – (F) show staining at the polymer-artery interface, revealing that endothelial cells exist in the vessels formed from the treatment. (G) – (I) focus on just the native artery for the polymer + peptide treated group, illustrating a thin endothelial lining along the intima and lining of white blood cells along the artery wall. The untreated group (J) – (L) portrays a diseased endothelial lining representative of ischemic or occluded tissue (L), but similar lining of hematopoietic cells along the artery wall (K).

Appendix P: MATLAB Code for PCA

```
%Principal component analysis (PCA)

clc
clear all
clear all

%$$$Define variable values for each polymer examined
```

```
%Molar = x%PCL, rho = crosslinking density, Xg = gel content, Mn =
%number-average molecular weight, Mw = weight-average molecular weight, PDI
%= Mw/Mn or polydispersity index, Tm = melting temperature, Hm = enthalphy
%of fusion, Tc = crystallization temperature, Hc = enthalpy of
%crystallizaiton, Est = storage modulus at 37 Celsius, Etn = tensile
%modulus at 37 Celsius, Snmax = strain at break, Ssmax = stress at break,
%Rf = shape fixity, Rr = shape recovery, e1 = stain from fixing at 0.039
%MPa, Rr1 = shape recovery after first cycle
Molar = [100, 95.84, 95.84 94.26, 91.96, 89.42, 89.42, 88.8, 88.44, 85.5]';
rho = [0.04916 .03023 .03073 .01731 .01531 .01821 .003541 .007373 .01661 .0038]';
Xg = [72 36.7 63 60.3 73.2 49 78.2 71.2 64.1 50.3]';
Mn = [11300, 15060 15060, 16546, 22026, 13627, 13627 29709, 19087 12095]';
Mw = [17368 26870 26870 39050 35074 34049 34049 48842 36430 28931]';
PDI = [1.54 1.78 1.78 2.36 1.59 2.5 2.5 1.64 1.91 2.39]';
Tm = [48 45.4 43.4 37.9 39 37.9 27.5 35.1 33.4 29.7]';
Hm = [48.2 50.9 44.6 39.1 35.3 38.7 19.7 31.2 33.7 28.3]';
Tc = [19.5 18.6 15.8 2.4 5.3 -2.1 -10 -6.1 -8.7 -13.9]';
Hc = [48.6 50.2 43.2 38.7 35.3 36.5 11.9 32.6 31.4 17.2]';
Est = [273 130 186.1 103.4 74.4 75.7 24.7 45.6 67.8 16.4]';
Etn = [83.8 75.9 55 4.9 18.6 4.53 3.08 5.44 4.24 2.2]';
Snmax = [8.48 39.8 93.4 253 353.4 131.4 101 300.2 84.5 28.1]';
Ssmax = [4.15 1.81 3.3 2.36 2.46 .77 .68 1.14 .99 .12]';
Rf = [98.3 99.8 94.2 98.7 98.7 99.8 92.5 99.1 98.8 99.6]';
Rr = [99.5 99.8 99.4 98.5 98.0 99.7 100 92.5 99 86.9]';
e1 = [14.1 122.1 9.6 8.27 6 40.8 6.2 7.8 14.6 7.1]';
Rr1 = [99.7 99.9 99.4 93.7 86.3 97.4 90.8 64.3 99.9 60.1]';

%n(row) x p(column) data matrix, with p being different variables and n being
%observations (i.e. polymers)
variables = [Molar rho Xg Mn Mw PDI Tm Hm Tc Hc Est Etn Snmax Ssmax Rf Rr e1 Rr1];

%define number of variables
n = length(variables);

%Create string matrix containing variable names
Varnames={'x%';'rho';'Xg';'Mn';'Mw';'PDI';'Tm';'Hm';'Tc';'Hc';...
    'Est';'Etn';'Snmax';'Ssmax';'Rf';'Rr';'e1';'Rr1'};

%Use princomp function to conduct principal component analysis
%coeff = princomp(x) performs PCA on the n-by-p matrix x
%coeff is a p-by-p matrix, with each column containing coefficients for one
%principal component
%princomp centers x by subtracting off column means, and
%princomp(zscore(x)) standardizes the variables, as they are in different
%units
%[Coeff,score] = princomp(x) returns the principal component scores (i.e. x
%represented in the principal component space. Rows are observations,
%columns correspond to components
%[Coeff,score, latent] = princomp(x) returns latent, a vector containing
%the eigenvalues of the covariance matrix x
%Variables are standardardized using zscore function

[pc,score,latent] = princomp(zscore(variables));

cumsum(latent)./sum(latent)
```

```
biplot(pc(:,1:2),'Scores',score(:,1:2),'VarLabels',Varnames);

CovMat = cov(zscore(variables));
[V,D]=eigs(CovMat,6);

figure(2);
imagesc(V);
% set(gca,'XTickLabel',Varnames);
set(gca,'Ytick',1:1:n,'YTickLabel',Varnames);
colorbar;

figure(3);
imagesc(CovMat);
set(gca,'Xtick',1:1:n,'XTickLabel',Varnames);
set(gca,'Ytick',1:1:n,'YTickLabel',Varnames);
colorbar;

figure(4);
biplot(pc(:,1:3),'Scores',score(:,1:3),'Varlabels',Varnames);
```

REFERENCES

1. Behl M, Lendlein A: **Shape-memory polymers.** *Materials Today* 2007, **10:**20-28.
2. Lendlein A, Jiang H, Junger O, Langer R: **Light-induced shape-memory polymers.** *Nature* 2005, **434:**879-882.
3. Wu L, Jin C, Sun X: **Synthesis, properties, and light-induced shape memory effect of multiblock polyesterurethanes containing biodegradable segments and pendant cinnamamide groups.** *Biomacromolecules* 2011, **12:**235-241.
4. Schmidt AM: **Electromagnetic activation of shape memory polymer networks containing magnetic nanoparticles.** *Macromolecular rapid communications* 2006, **27:**1168-1172.
5. Jung YC, Yoo HJ, Kim YA, Cho JW, Endo M: **Electroactive shape memory performance of polyurethane composite having homogeneously dispersed and covalently crosslinked carbon nanotubes.** *Carbon* 2010, **48:**1598-1603.
6. Sahoo NG, Jung YC, Cho JW: **Electroactive shape memory effect of polyurethane composites filled with carbon nanotubes and conducting polymer.** *Mater Manuf Process* 2007, **22:**419-423.
7. Huang WM, Yang B, An L, Li C, Chan YS: **Water-driven programmable polyurethane shape memory polymer: Demonstration and mechanism.** *Appl Phys Lett* 2005, **86**.
8. Mendez J, Annamalai PK, Eichhorn SJ, Rusli R, Rowan SJ, Foster EJ, Weder C: **Bioinspired Mechanically Adaptive Polymer Nanocomposites with Water-Activated Shape-Memory Effect.** *Macromolecules* 2011, **44:**6827-6835.
9. Han X-J, Dong Z-Q, Fan M-M, Liu Y, li J-H, Wang Y-F, Yuan Q-J, Li B-J, Zhang S: **pH-Induced Shape-Memory Polymers.** *Macromolecular rapid communications* 2012, **33:**1055-1060.
10. Ratna D, Karger-Kocsis J: **Recent advances in shape memory polymers and composites: a review.** *Journal of Materials Science* 2008, **43:**254-269.
11. Xu J, Song J: *Thermal Responsive Shape Memory Polymers for Biomedical Applications.* 2011.
12. Xie T: **Recent advances in polymer shape memory.** *Polymer* 2011, **52:**4985-5000.
13. Lendlein A, Langer R: **Biodegradable, Elastic Shape-Memory Polymers for Potential Biomedical Applications.** *Science* 2002, **296:**1673-1676.
14. Leng J, Lan X, Liu Y, Du S: **Shape-memory polymers and their composites: Stimulus methods and applications.** *Progress in Materials Science* 2011, **56:**1077-1135.
15. Lendlein A, Kelch S: **Shape-Memory Polymers.** *Angewandte Chemie International Edition* 2002, **41:**2034-2057.
16. Rousseau IA: **Challenges of shape memory polymers: A review of the progress toward overcoming SMP's limitations.** *Polymer Engineering & Science* 2008, **48:**2075-2089.
17. Bossi O, Gartsbein M, Leitges M, Kuroki T, Grossman S, Tennenbaum T: **UV irradiation increases ROS production via PKCdelta signaling in primary murine fibroblasts.** *Journal of cellular biochemistry* 2008, **105:**194-207.
18. He Z, Satarkar N, Xie T, Cheng Y-T, Hilt JZ: **Remote Controlled Multishape Polymer Nanocomposites with Selective Radiofrequency Actuations.** *Advanced Materials* 2011, **23:**3192-3196.
19. Xie T: **Tunable polymer multi-shape memory effect.** *Nature* 2010, **464:**267-270.
20. Tupper M, Munshi N, Beavers F, Gall K, Mikuls M, Jr., Meink T: **Developments in elastic memory composite materials for spacecraft deployable structures.** In *Aerospace Conference, 2001, IEEE Proceedings*; *2001*. 2001: 2541-2547 vol.2545.
21. Davis KA, Burke KA, Mather PT, Henderson JH: **Dynamic cell behavior on shape memory polymer substrates.** *Biomaterials* 2011, **32:**2285-2293.

22. Le DM, Kulangara K, Adler AF, Leong KW, Ashby VS: **Dynamic topographical control of mesenchymal stem cells by culture on responsive poly(epsilon-caprolactone) surfaces.** *Adv Mater* 2011, **23:**3278-3283.
23. Lendlein A, Behl M, Hiebl B, Wischke C: **Shape-memory polymers as a technology platform for biomedical applications.** *Expert review of medical devices* 2010, **7:**357-379.
24. Serrano MC, Ameer GA: **Recent Insights Into the Biomedical Applications of Shape-memory Polymers.** *Macromolecular bioscience* 2012**:**n/a-n/a.
25. Lendlein A, Langer R: **Biodegradable, elastic shape-memory polymers for potential biomedical applications.** *Science* 2002, **296:**1673-1676.
26. LANGER R, LENDLEIN A: **Biodegradable shape memory polymeric sutures.** In *Book Biodegradable shape memory polymeric sutures* (Editor ed.^eds.). City: WO Patent 2,003,088,818; 2003.
27. GORALTCHOUK A, LAI J, HERRMANN R: **SHAPE-MEMORY SELF-RETAINING SUTURES, METHODS OF MANUFACTURE, AND METHODS OF USE.** In *Book SHAPE-MEMORY SELF-RETAINING SUTURES, METHODS OF MANUFACTURE, AND METHODS OF USE* (Editor ed.^eds.). City: WO Patent 2,009,132,284; 2009.
28. Bettuchi M, Heinrich R: **NOVEL SURGICAL FASTENER.** In *Book NOVEL SURGICAL FASTENER* (Editor ed.^eds.). City: Google Patents; 2008.
29. Yakacki CM, Shandas R, Lanning C, Rech B, Eckstein A, Gall K: **Unconstrained recovery characterization of shape-memory polymer networks for cardiovascular applications.** *Biomaterials* 2007, **28:**2255-2263.
30. Baer GM, Wilson TS, Small W, Hartman J, Benett WJ, Matthews DL, Maitland DJ: **Thermomechanical properties, collapse pressure, and expansion of shape memory polymer neurovascular stent prototypes.** *Journal of Biomedical Materials Research Part B: Applied Biomaterials* 2009, **90:**421-429.
31. Yakacki CM, Shandas R, Lanning C, Gall K: **Free Recovery Effects of Shape-Memory Polymers for Cardiovascular Stents.** In *MRS Proceedings*. Cambridge Univ Press; 2005
32. Baer G, Small W, Wilson T, Benett W, Matthews D, Hartman J, Maitland D: **Fabrication and in vitro deployment of a laser-activated shape memory polymer vascular stent.** *Biomedical engineering online* 2007, **6:**43.
33. Baer GM, Wilson TS, Small Wt, Hartman J, Benett WJ, Matthews DL, Maitland DJ: **Thermomechanical properties, collapse pressure, and expansion of shape memory polymer neurovascular stent prototypes.** *Journal of biomedical materials research Part B, Applied biomaterials* 2009, **90:**421-429.
34. Metcalfe A, Desfaits AC, Salazkin I, Yahia L, Sokolowski WM, Raymond J: **Cold hibernated elastic memory foams for endovascular interventions.** *Biomaterials* 2003, **24:**491-497.
35. Hampikian JM, Heaton BC, Tong FC, Zhang Z, Wong C: **Mechanical and radiographic properties of a shape memory polymer composite for intracranial aneurysm coils.** *Materials Science and Engineering: C* 2006, **26:**1373-1379.
36. Simon P, Lendlein A, Schnitter B: **Stents for vascular or non-vascular applications by minimally invasive implantation include a biodegradable shape-memory polymer material.** In *Book Stents for vascular or non-vascular applications by minimally invasive implantation include a biodegradable shape-memory polymer material* (Editor ed.^eds.). City: DE Patent 10,357,747; 2005.
37. Simon P, Kratz K, Lendlein A, Schnitter B: **Stent of shape-memory polymer is used as vascular eg iliac, renal, carotid, femoral-poplietal or coronary stent or design non-vascular stent for gastrointestinal tract, trachea, esophagus, bile duct, ureter, urethra or Fallopian tube.** In *Book Stent of shape-memory polymer is used as vascular eg iliac, renal, carotid, femoral-poplietal or*

coronary stent or design non-vascular stent for gastrointestinal tract, trachea, esophagus, bile duct, ureter, urethra or Fallopian tube (Editor ed.^eds.). City: DE Patent 10,357,743; 2005.

38. Jordan G: **Shape memory polymeric stent.** In *Book Shape memory polymeric stent* (Editor ed.^eds.). City: Google Patents; 2008.
39. Xue L, Dai S, Li Z: **Biodegradable shape-memory block co-polymers for fast self-expandable stents.** *Biomaterials* 2010, **31:**8132-8140.
40. Chen M-C, Tsai H-W, Chang Y, Lai W-Y, Mi F-L, Liu C-T, Wong H-S, Sung H-W: **Rapidly self-expandable polymeric stents with a shape-memory property.** *Biomacromolecules* 2007, **8:**2774-2780.
41. Chen M-C, Chang Y, Liu C-T, Lai W-Y, Peng S-F, Hung Y-W, Tsai H-W, Sung H-W: **The characteristics and< i> in vivo</i> suppression of neointimal formation with sirolimus-eluting polymeric stents.** *Biomaterials* 2009, **30:**79-88.
42. Small W, Buckley PR, Wilson TS, Benett WJ, Hartman J, Saloner D, Maitland DJ: **Shape memory polymer stent with expandable foam: a new concept for endovascular embolization of fusiform aneurysms.** *Biomedical Engineering, IEEE Transactions on* 2007, **54:**1157-1160.
43. Maitland DJ, Metzger MF, Schumann D, Lee A, Wilson TS: **Photothermal properties of shape memory polymer micro-actuators for treating stroke*.** *Lasers in surgery and medicine* 2002, **30:**1-11.
44. Metcalfe A, Desfaits A-C, Salazkin I, Yahia LH, Sokolowski WM, Raymond J: **Cold hibernated elastic memory foams for endovascular interventions.** *Biomaterials* 2003, **24:**491-497.
45. Hartman J, Small W, Wilson T, Brock J, Buckley P, Benett W, Loge J, Maitland D: **Embolectomy in a rabbit acute arterial occlusion model using a novel electromechanical extraction device.** *American Journal of Neuroradiology* 2007, **28:**872-874.
46. Bellin I, Kelch S, Langer R, Lendlein A: **Polymeric triple-shape materials.** *Proceedings of the National Academy of Sciences of the United States of America* 2006, **103:**18043-18047.
47. Hartman J, Small Wt, Wilson TS, Brock J, Buckley PR, Benett WJ, Loge JM, Maitland DJ: **Embolectomy in a rabbit acute arterial occlusion model using a novel electromechanical extraction device.** *AJNR American journal of neuroradiology* 2007, **28:**872-874.
48. TEAGUE J: **Light responsive medical retrieval devices.** In *Book Light responsive medical retrieval devices* (Editor ed.^eds.). City: WO Patent 2,007,145,800; 2007.
49. Feldman T, Wang W: **Lumen occluders made from thermodynamic materials.** In *Book Lumen occluders made from thermodynamic materials* (Editor ed.^eds.). City: Google Patents; 2003.
50. SHANDAS R, YAKACKI C, NAIR D, GALL K, LYONS M: **Shape memory polymer-based transcervical device for permanent or temporary sterilization.** In *Book Shape memory polymer-based transcervical device for permanent or temporary sterilization* (Editor ed.^eds.). City: WO Patent 2,008,077,123; 2008.
51. Neffe AT, Hanh BD, Steuer S, Lendlein A: **Polymer networks combining controlled drug release, biodegradation, and shape memory capability.** *Advanced Materials* 2009, **21:**3394-3398.
52. Jordan G: **Shape Memory Polymeric Stent.** In *Book Shape Memory Polymeric Stent* (Editor ed.^eds.). City: US Patent App. 13/763,149; 2013.
53. Shadduck JH: **Implants for treating ocular hypertension, methods of use and methods of fabrication.** In *Book Implants for treating ocular hypertension, methods of use and methods of fabrication* (Editor ed.^eds.). City: Google Patents; 2004.
54. Sharp AA, Panchawagh HV, Ortega A, Artale R, Richardson-Burns S, Finch DS, Gall K, Mahajan RL, Restrepo D: **Toward a self-deploying shape memory polymer neuronal electrode.** *Journal of neural engineering* 2006, **3:**L23.
55. Ware T, Simon D, Arreaga-Salas DE, Reeder J, Rennaker R, Keefer EW, Voit W: **Fabrication of Responsive, Softening Neural Interfaces.** *Advanced functional materials* 2012, **22:**3470-3479.

56. Yakacki CM, Shandas R, Safranski D, Ortega AM, Sassaman K, Gall K: **Strong, Tailored, Biocompatible Shape-Memory Polymer Networks.** *Advanced functional materials* 2008, **18:**2428-2435.
57. Jung YC, Cho JW: **Application of shape memory polyurethane in orthodontic.** *Journal of Materials Science: Materials in Medicine* 2010, **21:**2881-2886.
58. Marco D, Eckhouse S: **Bioerodible self-deployable intragastric implants.** In *Book Bioerodible self-deployable intragastric implants* (Editor ed.^eds.). City: US Patent 20,070,156,248; 2007.
59. Marco D, Eckhouse S: **Bioerodible self-deployable intragastric implants.** In *Book Bioerodible self-deployable intragastric implants* (Editor ed.^eds.). City: Google Patents; 2010.
60. Lendlein A BM, Hiebl B, Wischke C: **Shape-memory polymers as a technology platform for biomedical applications.** *Expert review of medical devices* 2010, **7:**357-379.
61. Baer G, Wilson TS, Matthews DL, Maitland DJ: **Shape-memory behavior of thermally stimulated polyurethane for medical applications.** *Journal of applied polymer science* 2007, **103:**3882-3892.
62. Chen MC, Tsai HW, Chang Y, Lai WY, Mi FL, Liu CT, Wong HS, Sung HW: **Rapidly self-expandable polymeric stents with a shape-memory property.** *Biomacromolecules* 2007, **8:**2774-2780.
63. Chen MC, Chang Y, Liu CT, Lai WY, Peng SF, Hung YW, Tsai HW, Sung HW: **The characteristics and in vivo suppression of neointimal formation with sirolimus-eluting polymeric stents.** *Biomaterials* 2009, **30:**79-88.
64. Xue L, Dai S, Li Z: **Biodegradable shape-memory block co-polymers for fast self-expandable stents.** *Biomaterials* 2010, **31:**8132-8140.
65. Maitland DJ, Small Wt, Ortega JM, Buckley PR, Rodriguez J, Hartman J, Wilson TS: **Prototype laser-activated shape memory polymer foam device for embolic treatment of aneurysms.** *Journal of biomedical optics* 2007, **12:**030504.
66. Rodriguez J, Yu Y-J, Miller M, Wilson T, Hartman J, Clubb F, Gentry B, Maitland D: **Opacification of Shape Memory Polymer Foam Designed for Treatment of Intracranial Aneurysms.** *Annals of biomedical engineering* 2012, **40:**883-897.
67. Small Wt, Singhal P, Wilson TS, Maitland DJ: **Biomedical applications of thermally activated shape memory polymers.** *Journal of materials chemistry* 2010, **20:**3356-3366.
68. Maitland DJ, Metzger MF, Schumann D, Lee A, Wilson TS: **Photothermal properties of shape memory polymer micro-actuators for treating stroke.** *Lasers in surgery and medicine* 2002, **30:**1-11.
69. Small W, Singhal P, Wilson TS, Maitland DJ: **Biomedical applications of thermally activated shape memory polymers.** *Journal of materials chemistry* 2010, **20:**3356-3366.
70. Nagahama K, Ueda Y, Ouchi T, Ohya Y: **Biodegradable Shape-Memory Polymers Exhibiting Sharp Thermal Transitions and Controlled Drug Release.** *Biomacromolecules* 2009, **10:**1789-1794.
71. Neffe AT, Hanh BD, Steuer S, Lendlein A: **Polymer Networks Combining Controlled Drug Release, Biodegradation, and Shape Memory Capability.** *Advanced Materials* 2009, **21:**3394-3398.
72. Serrano MC, Carbajal L, Ameer GA: **Novel Biodegradable Shape-Memory Elastomers with Drug-Releasing Capabilities.** *Advanced Materials* 2011, **23:**2211-2215.
73. Wischke C, Neffe AT, Lendlein A: **Controlled drug release from biodegradable shape-memory polymers.** In *Shape-Memory Polymers.* Springer; 2010: 177-205
74. Wischke C, Neffe AT, Steuer S, Lendlein A: **Evaluation of a degradable shape-memory polymer network as matrix for controlled drug release.** *Journal of Controlled Release* 2009, **138:**243-250.
75. Liu C, Qin H, Mather PT: **Review of progress in shape-memory polymers.** *Journal of materials chemistry* 2007, **17**.

76. Linfante I, Andreone V, Akkawi N, Wakhloo AK: **Internal Carotid Artery Stenting in Patients over 80 Years of Age: Single-Center Experience and Review of the Literature.** *Journal of Neuroimaging* 2009, **19:**158-163.
77. Brott TG, Hobson RW, Howard G, Roubin GS, Clark WM, Brooks W, Mackey A, Hill MD, Leimgruber PP, Sheffet AJ, et al: **Stenting versus Endarterectomy for Treatment of Carotid-Artery Stenosis.** *New England Journal of Medicine* 2010, **363:**11-23.
78. Walker MD, Marler JR, Goldstein M, et al.: **ENdarterectomy for asymptomatic carotid artery stenosis.** *JAMA : the journal of the American Medical Association* 1995, **273:**1421-1428.
79. Abbott AL: **Medical (Nonsurgical) Intervention Alone Is Now Best for Prevention of Stroke Associated With Asymptomatic Severe Carotid Stenosis: Results of a Systematic Review and Analysis.** *Stroke; a journal of cerebral circulation* 2009, **40:**e573-e583.
80. Erickson KM, Cole DJ: **Carotid artery disease: stenting vs endarterectomy.** *British Journal of Anaesthesia* 2010, **105:**i34-i49.
81. Maldonado TS: **What are Current Preprocedure Imaging Requirements for Carotid Artery Stenting and Carotid Endarterectomy: Have Magnetic Resonance Angiography and Computed Tomographic Angiography Made a Difference?** *Seminars in Vascular Surgery* 2007, **20:**205-215.
82. Lauder C, Kelly A, Thompson MM, London NJM, Bell PRF, Naylor AR: **Early and late outcome after carotid artery bypass grafting with saphenous vein.** *Journal of Vascular Surgery* 2003, **38:**1025-1030.
83. Houkin K, Kamiyama H, Kuroda S, Ishikawa T, Takahashi A, Abe H: **Long-term patency of radial artery graft bypass for reconstruction of the internal carotid artery.** *Journal of neurosurgery* 1999, **90:**786-790.
84. Zhou W, Lin PH, Bush RL, Peden E, Guerrero MA, Terramani T, Lubbe DF, Nguyen L, Lumsden AB: **Carotid artery aneurysm: Evolution of management over two decades.** *Journal of Vascular Surgery* 2006, **43:**493-496.
85. Head SJ, Börgermann J, Osnabrugge RLJ, Kieser TM, Falk V, Taggart DP, Puskas JD, Gummert JF, Kappetein AP: **Coronary artery bypass grafting: Part 2—optimizing outcomes and future prospects.** *European heart journal* 2013, **34:**2873-2886.
86. Kakisis JD, Liapis CD, Breuer C, Sumpio BE: **Artificial blood vessel: the Holy Grail of peripheral vascular surgery.** *Journal of Vascular Surgery* 2005, **41:**349-354.
87. Brewster LP, Bufallino D, Ucuzian A, Greisler HP: **Growing a living blood vessel: insights for the second hundred years.** *Biomaterials* 2007, **28:**5028-5032.
88. Place ES, Evans ND, Stevens MM: **Complexity in biomaterials for tissue engineering.** *Nature materials* 2009, **8:**457-470.
89. Woodruff MA, Hutmacher DW: **The return of a forgotten polymer—polycaprolactone in the 21st century.** *Progress in Polymer Science* 2010, **35:**1217-1256.
90. Pektok E, Nottelet B, Tille J-C, Gurny R, Kalangos A, Moeller M, Walpoth BH: **Degradation and Healing Characteristics of Small-Diameter Poly (ε-Caprolactone) Vascular Grafts in the Rat Systemic Arterial CirculationCLINICAL PERSPECTIVE.** *Circulation* 2008, **118:**2563-2570.
91. Zachman AL, Crowder SW, Ortiz O, Zienkiewicz KJ, Bronikowski CM, Yu SS, Giorgio TD, Guelcher SA, Kohn J, Sung H-J: **Pro-angiogenic and anti-inflammatory regulation by functional peptides loaded in polymeric implants for soft tissue regeneration.** *Tissue Engineering Part A* 2012, **19:**437-447.
92. Neuss S, Blomenkamp I, Stainforth R, Boltersdorf D, Jansen M, Butz N, Perez-Bouza A, Knuchel R: **The use of a shape-memory poly(epsilon-caprolactone)dimethacrylate network as a tissue engineering scaffold.** *Biomaterials* 2009, **30:**1697-1705.
93. Jeong HM, Kim BK, Choi YJ: **Synthesis and properties of thermotropic liquid crystalline polyurethane elastomers.** *Polymer* 2000, **41:**1849-1855.

94. Takao A, Fusae M, Yu N: **Preparation of cross-linked aliphatic polyester and application to thermo-responsive material.** *Journal of Controlled Release* 1994, **32:**87-96.
95. Uto K, Yamamoto K, Hirase S, Aoyagi T: **Temperature-responsive cross-linked poly(ε-caprolactone) membrane that functions near body temperature.** *Journal of Controlled Release* 2006, **110:**408-413.
96. Muroya T, Yamamoto K, Aoyagi T: **Degradation of cross-linked aliphatic polyester composed of poly(ε-caprolactone-co-d,l-lactide) depending on the thermal properties.** *Polymer Degradation and Stability* 2009, **94:**285-290.
97. Ebara M, Uto K, Idota N, Hoffman JM, Aoyagi T: **Shape-Memory Surface with Dynamically Tunable Nano-Geometry Activated by Body Heat.** *Advanced Materials* 2012, **24:**273-278.
98. Mahmud A, Xiong X-B, Lavasanifar A: **Novel Self-Associating Poly(ethylene oxide)-block-poly(ε-caprolactone) Block Copolymers with Functional Side Groups on the Polyester Block for Drug Delivery.** *Macromolecules* 2006, **39:**9419-9428.
99. Karikari AS, Edwards WF, Mecham JB, Long TE: **Influence of Peripheral Hydrogen Bonding on the Mechanical Properties of Photo-Cross-Linked Star-Shaped Poly(d,l-lactide) Networks.** *Biomacromolecules* 2005, **6:**2866-2874.
100. Pitt CG, Chasalow FI, Hibionada YM, Klimas DM, Schindler A: **Aliphatic Polyesters .1. The Degradation of Poly(Epsilon-Caprolactone) Invivo.** *Journal of applied polymer science* 1981, **26:**3779-3787.
101. Preston J, Mark H, Bikales N, Overberger C, Menges G: **Encyclopedia of Polymer Science and Technology.** *Mark, HF* 1988**:**381.
102. Sperling LH: *Introduction to physical polymer science.* Wiley. com; 2005.
103. Lancaster MV, Fields RD: **Antibiotic and cytotoxic drug susceptibility assays using resazurin and poising agents.** In *Book Antibiotic and cytotoxic drug susceptibility assays using resazurin and poising agents* (Editor ed.^eds.). City: Google Patents; 1996.
104. Hu X, Chen X, Liu S, Shi Q, Jing X: **Novel aliphatic poly (ester-carbonate) with pendant allyl ester groups and its folic acid functionalization.** *Journal of Polymer Science Part A: Polymer Chemistry* 2008, **46:**1852-1861.
105. Ortega AM, Kasprzak SE, Yakacki CM, Diani J, Greenberg AR, Gall K: **Structure–property relationships in photopolymerizable polymer networks: Effect of composition on the crosslinked structure and resulting thermomechanical properties of a (meth) acrylate-based system.** *Journal of applied polymer science* 2008, **110:**1559-1572.
106. Safranski DL, Smith KE, Gall K: **Mechanical Requirements of Shape-Memory Polymers in Biomedical Devices.** *Polymer Reviews* 2013, **53:**76-91.
107. Sauter T, Heuchel M, Kratz K, Lendlein A: **Quantifying the Shape-Memory Effect of Polymers by Cyclic Thermomechanical Tests.** *Polymer Reviews* 2013, **53:**6-40.
108. Lim Soo P, Luo L, Maysinger D, Eisenberg A: **Incorporation and release of hydrophobic probes in biocompatible polycaprolactone-block-poly (ethylene oxide) micelles: implications for drug delivery.** *Langmuir : the ACS journal of surfaces and colloids* 2002, **18:**9996-10004.
109. Serrano M, Pagani R, Vallet-Regı M, Pena J, Ramila A, Izquierdo I, Portoles M: **In vitro biocompatibility assessment of poly (< i> ε</i>-caprolactone) films using L929 mouse fibroblasts.** *Biomaterials* 2004, **25:**5603-5611.
110. Mani G, Feldman MD, Patel D, Agrawal C: **Coronary stents: a materials perspective.** *Biomaterials* 2007, **28:**1689-1710.